Measurement of the Quark and Gluon Fragmentation Functions in Z^0 Hadronic Decays

P. Abreu, W. Adam, T. Adye, I. Ajinenko, G D. Alekseev, R. Alemany, P P. Allport, S. Almehed, S. Amato, P. Andersson, et al.

EUROPEAN ORGANIZATION FOR NUCLEAR RESEARCH

CERN–PPE/97–108

8 August 1997

Measurement of the Quark and Gluon Fragmentation Functions in Z^0 Hadronic Decays

DELPHI Collaboration

Abstract

The transverse, longitudinal and asymmetric components of the fragmentation function are measured from the inclusive charged particles produced in e^+e^- collisions at LEP. As in deep inelastic scattering, these data are important for tests of QCD. The transverse σ_T and longitudinal σ_L components of the total hadronic cross section σ_{tot} are evaluated from the measured fragmentation functions. They are found to be $\sigma_T/\sigma_{tot} = 0.949 \pm 0.001(stat.) \pm 0.007(syst.)$ and $\sigma_L/\sigma_{tot} = 0.051 \pm 0.001(stat.) \pm 0.007(syst.)$ respectively. The strong coupling constant is calculated from σ_L/σ_{tot} in next-to-leading order of perturbative QCD, giving

$$\alpha_s(M_Z) = 0.120 \pm 0.002(stat.) \pm 0.013(syst.) \pm 0.007(scale) \ .$$

Including non-perturbative power corrections leads to

$$\alpha_s(M_Z) = 0.101 \pm 0.002(stat.) \pm 0.013(syst.) \pm 0.007(scale) \ .$$

The measured transverse and longitudinal components of the fragmentation function are used to estimate the mean charged multiplicity,

$$\langle n^{ch} \rangle = 21.21 \pm 0.01(stat.) \pm 0.20(syst.)$$

The fragmentation functions and multiplicities in $b\overline{b}$ and light quark events are compared. The measured transverse and longitudinal components of the fragmentation function allow the gluon fragmentation function to be evaluated.

(To be submitted to Zeit. f. Physik C)

P.Abreu[21], W.Adam[49], T.Adye[36], I.Ajinenko[41], G.D.Alekseev[16], R.Alemany[48], P.P.Allport[22], S.Almehed[24], U.Amaldi[9], S.Amato[46], P.Andersson[43], A.Andreazza[9], P.Antilogus[9], W-D.Apel[17], Y.Arnoud[14], B.Åsman[43], J-E.Augustin[25], A.Augustinus[30], P.Baillon[9], P.Bambade[19], F.Barao[21], M.Barbi[46], G.Barbiellini[45], D.Y.Bardin[16], G.Barker[9], A.Baroncelli[39], O.Barring[24], M.J.Bates[36], M.Battaglia[15], M.Baubillier[23], J.Baudot[38], K-H.Becks[51], M.Begalli[6], P.Beilliere[8], Yu.Belokopytov[9,52], K.Beloous[41], A.C.Benvenuti[5], C.Berat[14], M.Berggren[46], D.Bertini[25], D.Bertrand[2], M.Besancon[38], F.Bianchi[44], M.Bigi[44], M.S.Bilenky[16], P.Billoir[23], M-A.Bizouard[19], D.Bloch[10], M.Blume[51], M.Bonesini[27], W.Bonivento[27], M.Boonekamp[38], P.S.L.Booth[22], A.W.Borgland[4], G.Borisov[38,41], C.Bosio[39], O.Botner[47], E.Boudinov[30], B.Bouquet[19], C.Bourdarios[19], T.J.V.Bowcock[22], M.Bozzo[13], P.Branchini[39], K.D.Brand[35], T.Brenke[51], R.A.Brenner[47], R.C.A.Brown[9], P.Bruckman[18], J-M.Brunet[8], L.Bugge[32], T.Buran[32], T.Burgsmueller[51], P.Buschmann[51], S.Cabrera[48], M.Caccia[27], M.Calvi[27], A.J.Camacho Rozas[40], T.Camporesi[9], V.Canale[37], M.Canepa[13], F.Carena[9], L.Carroll[22], C.Caso[13], M.V.Castillo Gimenez[48], A.Cattai[9], F.R.Cavallo[5], V.Chabaud[9], Ph.Charpentier[9], L.Chaussard[25], P.Checchia[35], G.A.Chelkov[16], M.Chen[2], R.Chierici[44], P.Chliapnikov[41], P.Chochula[7], V.Chorowicz[25], J.Chudoba[29], V.Cindro[42], P.Collins[9], M.Colomer[48], R.Contri[13], E.Cortina[48], G.Cosme[19], F.Cossutti[45], J-H.Cowell[22], H.B.Crawley[1], D.Crennell[36], G.Crosetti[13], J.Cuevas Maestro[33], S.Czellar[15], J.Dahm[51], B.Dalmagne[19], G.Damgaard[28], P.D.Dauncey[36], M.Davenport[9], W.Da Silva[23], A.Deghorain[2], G.Della Ricca[45], P.Delpierre[26], N.Demaria[34], A.De Angelis[9], W.De Boer[17], S.De Brabandere[2], C.De Clercq[2], C.De La Vaissiere[23], B.De Lotto[45], A.De Min[35], L.De Paula[46], H.Dijkstra[9], L.Di Ciaccio[37], A.Di Diodato[37], A.Djannati[8], J.Dolbeau[8], K.Doroba[50], M.Dracos[10], J.Drees[51], K.-A.Drees[51], M.Dris[31], J-D.Durand[25,9], D.Edsall[1], R.Ehret[17], G.Eigen[4], T.Ekelof[47], G.Ekspong[43], M.Elsing[9], J-P.Engel[10], B.Erzen[42], E.Falk[24], G.Fanourakis[11], D.Fassouliotis[45], M.Feindt[9], P.Ferrari[27], A.Ferrer[48], S.Fichet[23], T.A.Filippas[31], A.Firestone[1], P.-A.Fischer[10], H.Foeth[9], E.Fokitis[31], F.Fontanelli[13], F.Formenti[9], B.Franek[36], A.G.Frodesen[4], R.Fruhwirth[49], F.Fulda-Quenzer[19], J.Fuster[48], A.Galloni[22], D.Gamba[44], M.Gandelman[46], C.Garcia[48], J.Garcia[40], C.Gaspar[9], U.Gasparini[35], Ph.Gavillet[9], E.N.Gazis[31], D.Gele[10], J-P.Gerber[10], L.Gerdyukov[41], R.Gokieli[50], B.Golob[42], P.Goncalves[21], G.Gopal[36], L.Gorn[1], M.Gorski[50], Yu.Gouz[44,52], V.Gracco[13], E.Graziani[39], C.Green[22], A.Grefrath[51], P.Gris[38], G.Grosdidier[19], K.Grzelak[50], S.Gumenyuk[41], M.Gunther[47], J.Guy[36], F.Hahn[9], S.Hahn[51], Z.Hajduk[18], A.Hallgren[47], K.Hamacher[51], F.J.Harris[34], V.Hedberg[24], R.Henriques[21], J.J.Hernandez[48], P.Herquet[2], H.Herr[9], T.L.Hessing[34], J.-M.Heuser[51], E.Higon[48], S-O.Holmgren[43], P.J.Holt[34], D.Holthuizen[30], S.Hoorelbeke[2], M.Houlden[22], J.Hrubec[49], K.Huet[2], K.Hultqvist[43], J.N.Jackson[22], R.Jacobsson[43], P.Jalocha[9], R.Janik[7], Ch.Jarlskog[24], G.Jarlskog[24], P.Jarry[38], B.Jean-Marie[19], E.K.Johansson[43], L.Jonsson[24], P.Jonsson[24], C.Joram[9], P.Juillot[10], M.Kaiser[17], F.Kapusta[23], K.Karafasoulis[11], E.Karvelas[11], S.Katsanevas[25], E.C.Katsoufis[31], R.Keranen[4], Yu.Khokhlov[41], B.A.Khomenko[16], N.N.Khovanski[16], B.King[22], N.J.Kjaer[30], O.Klapp[51], H.Klein[9], P.Kluit[30], D.Knoblauch[17], P.Kokkinias[11], M.Koratzinos[9], C.Kourkoumelis[3], O.Kouznetsov[16], M.Krammer[49], C.Kreuter[9], I.Kronkvist[24], Z.Krumstein[16], W.Krupinski[18], P.Kubinec[7], W.Kucewicz[18], K.Kurvinen[15], C.Lacasta[9], I.Laktineh[25], J.W.Lamsa[1], L.Lanceri[45], D.W.Lane[1], P.Langefeld[51], J-P.Laugier[38], R.Lauhakangas[15], G.Leder[49], F.Ledroit[14], V.Lefebure[2], C.K.Legan[1], A.Leisos[11], R.Leitner[29], J.Lemonne[2], G.Lenzen[51], V.Lepeltier[19], T.Lesiak[18], M.Lethuillier[38], J.Libby[34], D.Liko[9], A.Lipniacka[43], I.Lippi[35], B.Loerstad[24], J.G.Loken[34], J.M.Lopez[40], D.Loukas[11], P.Lutz[38], L.Lyons[34], J.MacNaughton[49], G.Maehlum[17], J.R.Mahon[6], A.Maio[21], T.G.M.Malmgren[43], V.Malychev[16], F.Mandl[49], J.Marco[40], R.Marco[40], B.Marechal[46], M.Margoni[35], J-C.Marin[9], C.Mariotti[9], A.Markou[11], C.Martinez-Rivero[33], F.Martinez-Vidal[48], S.Marti i Garcia[22], J.Masik[29], F.Matorras[40], C.Matteuzzi[27], G.Matthiae[37], M.Mazzucato[35], M.Mc Cubbin[22], R.Mc Kay[1], R.Mc Nulty[9], G.Mc Pherson[22], J.Medbo[47], C.Meroni[27], S.Meyer[17], W.T.Meyer[1], M.Michelotto[35], E.Migliore[44], L.Mirabito[25], W.A.Mitaroff[49], U.Mjoernmark[24], T.Moa[43], R.Moeller[28], K.Moenig[9], M.R.Monge[13], P.Morettini[13], H.Mueller[17], K.Muenich[51], M.Mulders[30], L.M.Mundim[6], W.J.Murray[36], B.Muryn[14,18], G.Myatt[34], T.Myklebust[32], F.Naraghi[14], F.L.Navarria[5], S.Navas[48], K.Nawrocki[50], P.Negri[27], W.Neumann[51], N.Neumeister[49], R.Nicolaidou[3], B.S.Nielsen[28], M.Nieuwenhuizen[30], V.Nikolaenko[10], M.Nikolenko[10,16], P.Niss[43], A.Nomerotski[35], A.Normand[22], A.Nygren[24], W.Oberschulte-Beckmann[17], V.Obraztsov[41], A.G.Olshevski[16], A.Onofre[21], R.Orava[15], G.Orazi[10], S.Ortuno[48], K.Osterberg[15], A.Ouraou[38], P.Paganini[19], M.Paganoni[9,27], S.Paiano[5], R.Pain[23], H.Palka[18], Th.D.Papadopoulou[31], K.Papageorgiou[11], L.Pape[9], C.Parkes[34], F.Parodi[13], U.Parzefall[22], A.Passeri[39], M.Pegoraro[35], L.Peralta[21], H.Pernegger[49], M.Pernicka[49], A.Perrotta[5], C.Petridou[45], A.Petrolini[13], M.Petrovyck[41], H.T.Phillips[36], G.Piana[13], F.Pierre[38], M.Pimenta[21], E.Piotto[35], T.Podobnik[34], O.Podobrin[9], M.E.Pol[6], G.Polok[18], P.Poropat[45], V.Pozdniakov[16], P.Privitera[37], N.Pukhaeva[16], A.Pullia[27], D.Radojicic[34], S.Ragazzi[27], H.Rahmani[31], P.N.Ratoff[20], A.L.Read[32], M.Reale[51], P.Rebecchi[9], N.G.Redaelli[27], M.Regler[49], D.Reid[9], R.Reinhardt[51], P.B.Renton[34], L.K.Resvanis[3], F.Richard[19], J.Ridky[12], G.Rinaudo[44], O.Rohne[32], A.Romero[44], P.Ronchese[35], L.Roos[23], E.I.Rosenberg[1], P.Rosinsky[7], P.Roudeau[19], T.Rovelli[5], V.Ruhlmann-Kleider[38], A.Ruiz[40], H.Saarikko[15], Y.Sacquin[38], A.Sadovsky[16], G.Sajot[14], J.Salt[48], M.Sannino[13], H.Schneider[17], U.Schwickerath[17], M.A.E.Schyns[51], G.Sciolla[44], F.Scuri[45], P.Seager[20], Y.Sedykh[16], A.M.Segar[34], A.Seitz[17], R.Sekulin[36], L.Serbelloni[37], R.C.Shellard[6], A.Sheridan[22], P.Siegrist[9,38], R.Silvestre[38], F.Simonetto[35], A.N.Sisakian[16], T.B.Skaali[32], N.Skatchkov[16], G.Smadja[25], N.Smirnov[41], O.Smirnova[24], G.R.Smith[36], A.Sokolov[41], O.Solovianov[41], R.Sosnowski[50], D.Souza-Santos[6], T.Spassov[21], E.Spiriti[39], P.Sponholz[51], S.Squarcia[13], D.Stampfer[9], C.Stanescu[39], S.Stanic[42], S.Stapnes[32], I.Stavitski[35], K.Stevenson[34], A.Stocchi[19], R.Strub[10], B.Stugu[4], M.Szczekowski[50], M.Szeptycka[50], T.Tabarelli[27], J.P.Tavernet[23], O.Tchikilev[41], F.Tegenfeldt[47], F.Terranova[27], J.Thomas[34], A.Tilquin[26],

J.Timmermans[30], L.G.Tkatchev[16], T.Todorov[10], S.Todorova[10], D.Z.Toet[30], A.Tomaradze[2], B.Tome[21], A.Tonazzo[27], L.Tortora[39], G.Transtromer[24], D.Treille[9], G.Tristram[8], A.Trombini[19], C.Troncon[27], A.Tsirou[9], M-L.Turluer[38], I.A.Tyapkin[16], M.Tyndel[36], S.Tzamarias[11], B.Ueberschaer[51], O.Ullaland[9], V.Uvarov[41], G.Valenti[5], E.Vallazza[45], G.W.Van Apeldoorn[30], P.Van Dam[30], W.K.Van Doninck[2], J.Van Eldik[30], A.Van Lysebetten[2], N.Vassilopoulos[34], G.Vegni[27], L.Ventura[35], W.Venus[36], F.Verbeure[2], M.Verlato[35], L.S.Vertogradov[16], D.Vilanova[38], P.Vincent[25], L.Vitale[45], E.Vlasov[41], A.S.Vodopyanov[16], V.Vrba[12], H.Wahlen[51], C.Walck[43], C.Weiser[17], A.M.Wetherell[9], D.Wicke[51], J.H.Wickens[2], M.Wielers[17], G.R.Wilkinson[9], W.S.C.Williams[34], M.Winter[10], T.Wlodek[19], J.Yi[1], K.Yip[34], O.Yushchenko[41], F.Zach[25], A.Zaitsev[41], A.Zalewska[9], P.Zalewski[50], D.Zavrtanik[42], E.Zevgolatakos[11], N.I.Zimin[16], G.C.Zucchelli[43], G.Zumerle[35]

[1] Department of Physics and Astronomy, Iowa State University, Ames IA 50011-3160, USA
[2] Physics Department, Univ. Instelling Antwerpen, Universiteitsplein 1, B-2610 Wilrijk, Belgium
and IIHE, ULB-VUB, Pleinlaan 2, B-1050 Brussels, Belgium
and Faculté des Sciences, Univ. de l'Etat Mons, Av. Maistriau 19, B-7000 Mons, Belgium
[3] Physics Laboratory, University of Athens, Solonos Str. 104, GR-10680 Athens, Greece
[4] Department of Physics, University of Bergen, Allégaten 55, N-5007 Bergen, Norway
[5] Dipartimento di Fisica, Università di Bologna and INFN, Via Irnerio 46, I-40126 Bologna, Italy
[6] Centro Brasileiro de Pesquisas Físicas, rua Xavier Sigaud 150, RJ-22290 Rio de Janeiro, Brazil
and Depto. de Física, Pont. Univ. Católica, C.P. 38071 RJ-22453 Rio de Janeiro, Brazil
and Inst. de Física, Univ. Estadual do Rio de Janeiro, rua São Francisco Xavier 524, Rio de Janeiro, Brazil
[7] Comenius University, Faculty of Mathematics and Physics, Mlynska Dolina, SK-84215 Bratislava, Slovakia
[8] Collège de France, Lab. de Physique Corpusculaire, IN2P3-CNRS, F-75231 Paris Cedex 05, France
[9] CERN, CH-1211 Geneva 23, Switzerland
[10] Institut de Recherches Subatomiques, IN2P3 - CNRS/ULP - BP20, F-67037 Strasbourg Cedex, France
[11] Institute of Nuclear Physics, N.C.S.R. Demokritos, P.O. Box 60228, GR-15310 Athens, Greece
[12] FZU, Inst. of Physics of the C.A.S. High Energy Physics Division, Na Slovance 2, 180 40, Praha 8, Czech Republic
[13] Dipartimento di Fisica, Università di Genova and INFN, Via Dodecaneso 33, I-16146 Genova, Italy
[14] Institut des Sciences Nucléaires, IN2P3-CNRS, Université de Grenoble 1, F-38026 Grenoble Cedex, France
[15] Helsinki Institute of Physics, HIP, P.O. Box 9, FIN-00014 Helsinki, Finland
[16] Joint Institute for Nuclear Research, Dubna, Head Post Office, P.O. Box 79, 101 000 Moscow, Russian Federation
[17] Institut für Experimentelle Kernphysik, Universität Karlsruhe, Postfach 6980, D-76128 Karlsruhe, Germany
[18] Institute of Nuclear Physics and University of Mining and Metalurgy, Ul. Kawiory 26a, PL-30055 Krakow, Poland
[19] Université de Paris-Sud, Lab. de l'Accélérateur Linéaire, IN2P3-CNRS, Bât. 200, F-91405 Orsay Cedex, France
[20] School of Physics and Chemistry, University of Lancaster, Lancaster LA1 4YB, UK
[21] LIP, IST, FCUL - Av. Elias Garcia, 14-1°, P-1000 Lisboa Codex, Portugal
[22] Department of Physics, University of Liverpool, P.O. Box 147, Liverpool L69 3BX, UK
[23] LPNHE, IN2P3-CNRS, Universités Paris VI et VII, Tour 33 (RdC), 4 place Jussieu, F-75252 Paris Cedex 05, France
[24] Department of Physics, University of Lund, Sölvegatan 14, S-22363 Lund, Sweden
[25] Université Claude Bernard de Lyon, IPNL, IN2P3-CNRS, F-69622 Villeurbanne Cedex, France
[26] Univ. d'Aix - Marseille II - CPP, IN2P3-CNRS, F-13288 Marseille Cedex 09, France
[27] Dipartimento di Fisica, Università di Milano and INFN, Via Celoria 16, I-20133 Milan, Italy
[28] Niels Bohr Institute, Blegdamsvej 17, DK-2100 Copenhagen 0, Denmark
[29] NC, Nuclear Centre of MFF, Charles University, Areal MFF, V Holesovickach 2, 180 00, Praha 8, Czech Republic
[30] NIKHEF, Postbus 41882, NL-1009 DB Amsterdam, The Netherlands
[31] National Technical University, Physics Department, Zografou Campus, GR-15773 Athens, Greece
[32] Physics Department, University of Oslo, Blindern, N-1000 Oslo 3, Norway
[33] Dpto. Fisica, Univ. Oviedo, Avda. Calvo Sotelo, S/N-33007 Oviedo, Spain, (CICYT-AEN96-1681)
[34] Department of Physics, University of Oxford, Keble Road, Oxford OX1 3RH, UK
[35] Dipartimento di Fisica, Università di Padova and INFN, Via Marzolo 8, I-35131 Padua, Italy
[36] Rutherford Appleton Laboratory, Chilton, Didcot OX11 OQX, UK
[37] Dipartimento di Fisica, Università di Roma II and INFN, Tor Vergata, I-00173 Rome, Italy
[38] CEA, DAPNIA/Service de Physique des Particules, CE-Saclay, F-91191 Gif-sur-Yvette Cedex, France
[39] Istituto Superiore di Sanità, Ist. Naz. di Fisica Nucl. (INFN), Viale Regina Elena 299, I-00161 Rome, Italy
[40] Instituto de Fisica de Cantabria (CSIC-UC), Avda. los Castros, S/N-39006 Santander, Spain, (CICYT-AEN96-1681)
[41] Inst. for High Energy Physics, Serpukov P.O. Box 35, Protvino, (Moscow Region), Russian Federation
[42] J. Stefan Institute, Jamova 39, SI-1000 Ljubljana, Slovenia and Department of Astroparticle Physics, School of Environmental Sciences, Kostanjeviska 16a, Nova Gorica, SI-5000 Slovenia,
and Department of Physics, University of Ljubljana, SI-1000 Ljubljana, Slovenia
[43] Fysikum, Stockholm University, Box 6730, S-113 85 Stockholm, Sweden
[44] Dipartimento di Fisica Sperimentale, Università di Torino and INFN, Via P. Giuria 1, I-10125 Turin, Italy
[45] Dipartimento di Fisica, Università di Trieste and INFN, Via A. Valerio 2, I-34127 Trieste, Italy
and Istituto di Fisica, Università di Udine, I-33100 Udine, Italy
[46] Univ. Federal do Rio de Janeiro, C.P. 68528 Cidade Univ., Ilha do Fundão BR-21945-970 Rio de Janeiro, Brazil
[47] Department of Radiation Sciences, University of Uppsala, P.O. Box 535, S-751 21 Uppsala, Sweden
[48] IFIC, Valencia-CSIC, and D.F.A.M.N., U. de Valencia, Avda. Dr. Moliner 50, E-46100 Burjassot (Valencia), Spain
[49] Institut für Hochenergiephysik, Österr. Akad. d. Wissensch., Nikolsdorfergasse 18, A-1050 Vienna, Austria
[50] Inst. Nuclear Studies and University of Warsaw, Ul. Hoza 69, PL-00681 Warsaw, Poland
[51] Fachbereich Physik, University of Wuppertal, Postfach 100 127, D-42097 Wuppertal, Germany
[52] On leave of absence from IHEP Serpukhov

1 Introduction

The study of the inclusive hadron production process $e^+e^- \to h + X$ provides a test of the QCD predictions on scaling violation effects in the fragmentation functions. These functions, $D^h_{q(g)}(x_p)$, where $x_p = 2p_h/Q$ with p_h and Q the hadron momentum and e^+e^- centre-of-mass energy respectively, describe the transition of the produced quarks (q) and gluons (g) to the final state hadrons (h). In the framework of QCD, the fragmentation functions obey DGLAP [1] evolution equations analogous to those used for describing the structure functions of deep-inelastic scattering. QCD analysis of the scaling violation effects in the fragmentation functions, performed on the basis of these equations, allows the value of α_s to be extracted [2–5], as in the structure function analysis of the process of deep-inelastic scattering.

A number of experiments [6] have studied the behaviour of the ratio of the longitudinal and transverse structure functions, F_L and F_T, in deep-inelastic scattering :

$$R(x) = \frac{F_L(x)}{F_T(x)} = \frac{F_2(x) - 2xF_1(x)}{2F_1(x)} \,, \tag{1}$$

where x is the Bjorken variable, which can be replaced by x_p in electron-positron annihilation. These experiments have shown that the value of $R(x)$ decreases rapidly with increasing x.

In contrast with all other structure functions $F_i(x),\ i = 1, 2, 3$, the longitudinal component F_L vanishes in the parton model and is non-zero only in the framework of QCD, where it is proportional to α_s [7–9], thus being strongly connected with the structure of perturbative QCD.

In analogy with the structure functions, the corresponding inclusive cross-section components in e^+e^- annihilation are also important for perturbation theory. Particularly interesting are the second moments of the fragmentation functions, which can be calculated up to corrections suppressed by some power of Λ/Q, where Λ is the QCD scale parameter.

Important information for studies of the scaling violation effects and on the shapes of the quark and gluon distributions comes from the region of small x_p. In this region, the effects caused by the contribution of the longitudinal component of the fragmentation function become very important.

Measurements of the longitudinal component of the fragmentation function, $F_L(x_p)$, in inclusive charged hadron production, $e^+e^- \to h + X$, were performed by the TASSO collaboration [10] at centre-of-mass energies of 14 GeV, 22 GeV and 34 GeV. Due to the limited number of events, those results gave only a qualitative description of the behaviour of F_L. It was shown that F_L appears to be different from zero only at values of $x_p \leq 0.2$. Similar results were found by DELPHI on the basis of the preliminary analysis of 1991 data [11], where only the ratio of the longitudinal and transverse components was obtained. Measurements of the F_L and F_T fragmentation functions were also published recently by the OPAL and ALEPH collaborations [12,13].

The study of the different components of the fragmentation function in inclusive charged hadron production is performed here using the 1992-1993 DELPHI data. The present approach allows the transverse, longitudinal and asymmetric components of the quark fragmentation function to be measured and the corresponding components of the cross-section to be extracted. Using the value of the longitudinal cross-section obtained, together with next-to-leading order perturbative QCD calculations, the value of the strong coupling constant is evaluated. Finally, the gluon fragmentation function is estimated in the leading order QCD framework.

In the following, Section 2 describes the procedure of hadronic event selection with the DELPHI detector. Section 3 presents the evaluation method for the fragmentation function components and the results obtained. Section 4 is devoted to the calculation of the strong coupling constant. Studies of systematic effects are presented in Section 5. In Section 6 analysis of fragmentation function components in flavour-tagged events is discussed. Extraction of the gluon fragmentation function from F_T and F_L is described in Section 7.

2 Data selection

Data collected by the DELPHI detector in 1992-1993 at centre-of-mass energies around $\sqrt{s} = 91.2$ GeV ($86.2 \leq \sqrt{s} \leq 94.2$ GeV) were used. The detector and its performance are described in detail in [14,15].

Only charged particles in hadronic events were used. In the barrel region they were measured by a set of cylindrical tracking detectors in the solenoidal magnetic field of 1.2 T. The main tracking device was the Time Projection Chamber (TPC), which was cylindrical with a length of 3 m, an inner radius of 30 cm and an outer radius of 122 cm. Up to 16 space points were used for charged particle reconstruction. The space precision was about $\sigma_{R\varphi} = 250\,\mu$m and $\sigma_z = 880\,\mu$m [†].

Additional $R\varphi$ measurements were provided by the Outer Detector (OD) and the Inner Detector (ID). The OD was a cylindrical detector composed of drift tubes and situated at radii between 197 cm and 206 cm; its precision in $R\varphi$ was about $\pm 110\,\mu$m. The ID was a cylindrical drift chamber having an inner radius of 12 cm and an outer radius of 28 cm; its precision in $R\varphi$ was $\pm 90\,\mu$m.

In order to tag $Z^0 \to b\overline{b}$ events, the micro-vertex detector (VD) was used. It was located between the beam pipe and the ID and consisted of three concentric layers of silicon micro-strip detectors. The precision in $R\varphi$ was about $\pm 8\,\mu$m.

In the forward direction (θ between 11° and 33° and between 147° and 169°) charged particles were measured by a set of planar drift chambers, FCA and FCB.

The momentum resolution of the tracking system in the barrel region was

$$\sigma(1/p) = 0.57 \times 10^{-3} (\mathrm{GeV}/c)^{-1}$$

and in the forward region

$$\sigma(1/p) = 1.31 \times 10^{-3} (\mathrm{GeV}/c)^{-1} \ .$$

Each charged particle was required to pass the following selection criteria :

1. particle momentum between 0.1 GeV/c and 50 GeV/c;
2. measured track length above 50 cm;
3. polar angle between 11° and 169°;
4. impact parameter with respect to the beam crossing point below 5 cm in the transverse plane and below 10 cm along the beam axis.

Hadronic events were then selected by requiring :

1. at least 5 charged particles detected with momenta above 0.2 GeV/c;
2. total energy of all charged particles detected above 15 GeV (assuming the $\pi^{\pm}$ mass for the particles);

[†] The DELPHI coordinate system has the z axis aligned along the electron beam direction, the $R\varphi$-plane is perpendicular to it, and θ is the angle between the momentum of the particle and the axis of the e^- beam.

3. polar angle of the sphericity axis between 26° and 154°;
4. total energy of charged particles in each of the forward and backward hemispheres with respect to the sphericity axis above 3 GeV;
5. missing momentum below 20 GeV/c.

In total, 1,055,932 hadronic events were selected.

Only two variables, the fractional momentum x_p and $\cos\theta$ of each charged particle, were used for the analysis. In each x_p and $\cos\theta$ bin, the value of

$$f(x_p, \cos\theta) \equiv \frac{1}{N} \frac{n}{\Delta x_p \Delta \cos\theta} \tag{2}$$

was obtained, where N is the total number of hadronic events and n is the number of particles in a bin of width Δx_p by $\Delta\cos\theta$. The number and widths of the x_p intervals were chosen in order to provide a reasonable number of entries in each. Thus the full range $0 < x_p < 1$ was split into 22 intervals (see Table 1). For the $\cos\theta$ variable, 40 equidistant intervals in the range $-1 < \cos\theta < 1$ were used.

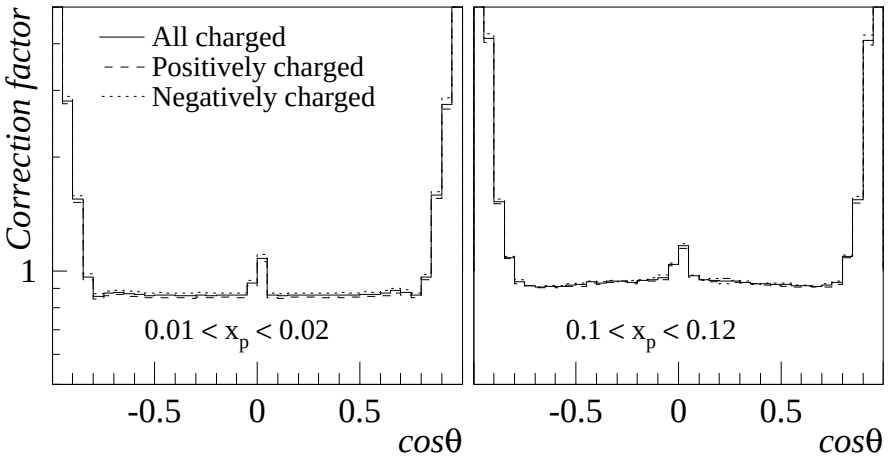

Figure 1: Correction factors for the polar angle distribution of charged particles in two different x_p intervals.

These normalized distributions were corrected for the detector acceptance and efficiency, for the kinematical cuts, and for the initial state radiation. The correction factor values

$$C(x_p, \cos\theta) = \frac{f(x_p, \cos\theta)_{true}}{f(x_p, \cos\theta)_{reconstructed}} \tag{3}$$

are shown in Fig. 1 as a function of $\cos\theta$ for two different bins of x_p. The values of $C(x_p, \cos\theta)$ were obtained by analysing events generated with the JETSET 7.3 PS program [16] with parameters taken from the DELPHI tuning [17]. Here $f(x_p, \cos\theta)_{true}$ is the distribution obtained from the final state hadrons in generated events, and $f(x_p, \cos\theta)_{reconstructed}$ represents the same distribution after full simulation of the response of the DELPHI detector [15] and application of the charged particle reconstruction and analysis procedures in the same way as for the real data. For the analysis of the charge asymmetric fragmentation function (see below), the distributions of positive and negative charged particles were obtained separately by using respective correction factors.

3 Components of the fragmentation function

The double-differential total cross-section for producing a charged hadron h in the process $e^+e^- \to h + X$ via the s-channel exchange of a virtual photon or Z^0 follows from the standard tensor analysis [8,18] :

$$\frac{d^2\sigma^h}{dx_p\, d\cos\theta} = \frac{3}{8}(1+\cos^2\theta)\frac{d\sigma_T^h}{dx_p} + \frac{3}{4}\sin^2\theta\frac{d\sigma_L^h}{dx_p} + \frac{3}{4}\cos\theta\frac{d\sigma_A^h}{dx_p} \ , \tag{4}$$

where $d\sigma_T^h/dx_p$, $d\sigma_L^h/dx_p$ and $d\sigma_A^h/dx_p$ are the transverse, longitudinal and asymmetric components of the differential cross-section, respectively.

In the present analysis, all kinds of charged hadrons have been taken into account. Therefore the overall charged hadron differential cross-sections $d\sigma_T^{ch}/dx_p$, $d\sigma_L^{ch}/dx_p$ and $d\sigma_A^{ch}/dx_p$ were measured :

$$\frac{d\sigma_P^{ch}}{dx_p} = \sum_h \frac{d\sigma_P^h}{dx_p} \ , \tag{5}$$

where the subscript P stands for T, L or A.

With the available number of events, it is possible to measure these components separately by weighting the double-differential total cross-sections :

$$\frac{d\sigma_P^{ch}}{dx_p} = \int_{-v}^{+v} W_P(\cos\theta, v)\left[\frac{d^2\sigma^{ch}}{dx_p\, d\cos\theta}\right] d\cos\theta \tag{6}$$

with appropriate weighting functions W_P ($P = T, L, T+L$, or A) [18] :

$$\begin{aligned} W_T(\cos\theta, v) &= [5\cos^2\theta(3-v^2) - v^2(5-3v^2)]/2v^5 \ , \\ W_L(\cos\theta, v) &= [v^2(5+3v^2) - 5\cos^2\theta(3+v^2)]/4v^5 \ , \\ W_{T+L}(\cos\theta, v) &= W_T(\cos\theta, v) + W_L(\cos\theta, v) \ , \\ W_A(\cos\theta, v) &= 2\cos\theta/v^3 \ , \end{aligned} \tag{7}$$

where the variable v delimits the absolute value of the cosine of the angular range used. In the present analysis, its value was taken as $v = 0.8$ in order to cover the interval where the correction factors are approximately constant (see Fig. 1). The effects of varying this value are taken into account in the systematic uncertainties.

A fitting procedure can also be used for the analysis of the distribution (4), as was done in [10–12]. The results obtained by the two methods are compared below.

Following [18], the transverse, longitudinal and asymmetric fragmentation functions are defined as :

$$F_P(x_p) \equiv \frac{1}{\sigma_{tot}}\frac{d\sigma_P^{ch}}{dx_p} \ , \tag{8}$$

where $P = T, L, A$, and σ_{tot} is the total hadronic cross-section. In the parton model limit ($\alpha_s \to 0$), the longitudinal fragmentation function $F_L(x_p)$ is equal to zero (by analogy with the longitudinal structure function in deep-inelastic scattering) and the transverse fragmentation function $F_T(x_p)$ coincides with the quark fragmentation function.

The asymmetric component, defined as above without reference to the hadron charge, should be zero. But separate analysis of positive and negative charged hadron samples should show a difference in sign between $d\sigma_A^{h^+}/dx_p$ and $d\sigma_A^{h^-}/dx_p$, where the superscripts h^+ and h^- denote the components of the fragmentation function for positively and negatively charged hadrons, respectively. The difference

$$\tilde{F}_A(x_p) = \frac{1}{\sigma_{tot}}\left(\frac{d\sigma_A^{h^+}}{dx_p} - \frac{d\sigma_A^{h^-}}{dx_p}\right) \tag{9}$$

is therefore used, following [18], to define the "charge asymmetric" fragmentation function. Since hadrons with sufficiently high x_p mainly result from the primary quark fragmentation, they carry the information on the primary quark charge. Therefore a non-zero charge asymmetric fragmentation function $\tilde{F}_A$ should be observed in this x_p region, reflecting the forward-backward asymmetry in the primary $e^+e^- \to q\bar{q}$ process.

3.1 Longitudinal and transverse fragmentation functions

The values for F_L and F_T found from this analysis are presented in Table 1 and are shown in Fig. 2, together with those of a similar analysis of JETSET 7.3 PS distributions and the corresponding results of OPAL [12].

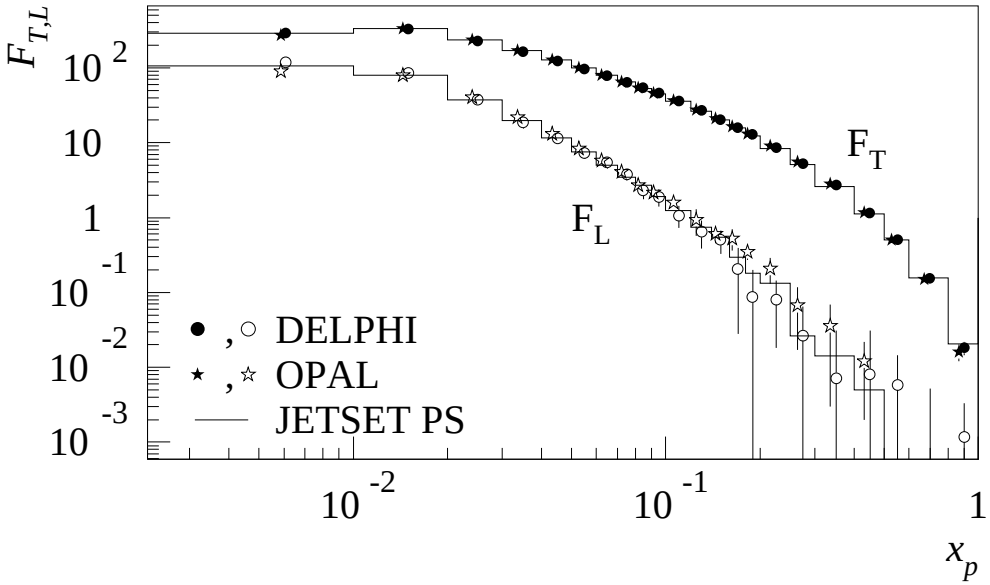

Figure 2: Measured values of F_L and F_T obtained by the weighting method in DELPHI (circles). Also shown are analogous OPAL data (stars, slightly shifted in x_p for clarity) and simulated JETSET PS distributions with the DELPHI tuning (histograms). Data are presented with total (statistical and systematic) errors.

Part of the difference in F_L between the DELPHI and OPAL data in the region $x_p < 0.02$ is due to the use of the x_E variable in OPAL rather than x_p here. Another difference is that OPAL used fits to angular distributions according to formula (4) rather than weighting.

Comparison of JETSET distributions generated with and without DELPHI tuning shows that differences in F_T (as well as in F_L) exist only in the region $x_p < 0.1$, and drop rapidly from 8% at $x_p < 0.01$ to 2% at $0.03 < x_p < 0.05$.

The sum of the transverse and longitudinal fragmentation functions can be evaluated by direct integration of the double-differential cross-section with the weight $(W_T + W_L)$ in the angular range $|\cos\theta| < v$. The result of such an integration, F_{T+L} for $v = 0.8$, is shown in Table 1. The statistical and systematic errors on F_{T+L} are reduced because F_T and F_L are anti-correlated. The ratios of the transverse σ_T^{ch} or longitudinal σ_L^{ch} cross-sections to the total cross-section σ_{tot} are obtained by integrating the corresponding fragmentation function :

$$\frac{\sigma_P^{ch}}{\sigma_{tot}} = \int_0^1 \frac{x_p}{2} F_P(x_p) dx_p \ , \qquad (10)$$

where $P = T, L$. This equation follows from the energy conservation sum rule and leads to the obvious equation $\sigma_T/\sigma_{tot} + \sigma_L/\sigma_{tot} = 1$ for all hadrons. Values of $\sigma_T^{ch}/\sigma_{tot}$ and $\sigma_L^{ch}/\sigma_{tot}$ are shown in the bottom line of Table 1.

The charged particle multiplicity can be obtained by integrating F_{T+L}. This gives

$$\langle n^{ch} \rangle = \int_0^1 F_{T+L} dx_p = 21.21 \pm 0.01(stat.) \pm 0.20(syst.). \tag{11}$$

The systematic uncertainty for $\langle n^{ch} \rangle$ was estimated by analysing the corresponding uncertainties of the fragmentation functions, as presented in Section 5 (see Table 4). The value of $\langle n^{ch} \rangle$ obtained is in good agreement with the average LEP/SLC result 20.99 ± 0.14 [19]. Charged particles with momentum below 0.1 GeV were taken into account through the standard correction factors (3), as were particles produced in secondary interactions. Charged hadrons produced in decays of K_s^0 and Λ are included, as is the usual convention, since the correction procedure considers them as unstable particles. The problem of particle reconstruction inefficiency in the forward regions of the detector was avoided, since the weighting functions W_T and W_L take into account the limited angular range used, effectively performing the extrapolation of the angular distributions to their edges.

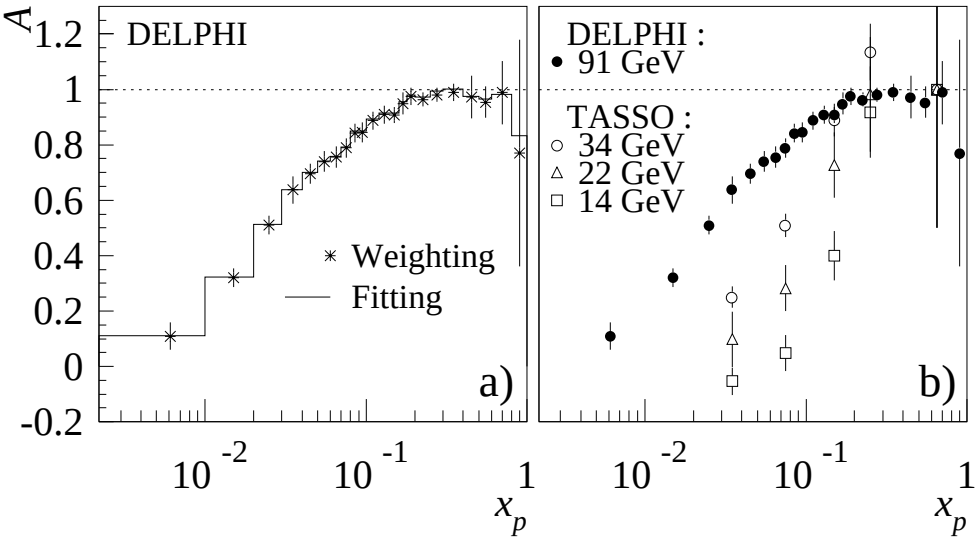

Figure 3: Comparison of $A = (F_T - 2F_L)/(F_T + 2F_L)$ calculated from the DELPHI data by the weighting method with other results : **a)** from DELPHI by applying the fitting method to the same data sample ; **b)** from TASSO at lower centre-of-mass energies. The combined statistical and systematic errors are shown for the DELPHI results.

The values of F_T and F_L have also been used to calculate the ratio $A = (F_T - 2F_L)\,/\,(F_T + 2F_L)$, which is simply connected to the double-differential cross-section (4) in the limit of a negligible asymmetric component :

$$\frac{d^2\sigma^{ch}}{dx_p\, d\cos\theta} \sim 1 + A\cos^2\theta \ . \tag{12}$$

Another way to determine A is by a direct fit of the angular distribution to equation (12), as done previously by TASSO [10] and DELPHI [11]. In Fig. 3a, the values of A obtained by the two methods are plotted as a function of x_p. The fit result generally slightly exceeds that from weighting; but they both behave very similarly, confirming

the theoretical expectation that the longitudinal contribution should be significant in the region of $x_p < 0.2$.

In Fig. 3b, values of A obtained with the weighting method are plotted together with the TASSO results at centre-of-mass energies of 14 GeV, 22 GeV and 34 GeV [10]. The energy dependence of A from TASSO is confirmed by the new precise DELPHI data. The DELPHI results provide a much better description of the A behaviour in the full x_p interval and clearly indicate the region where F_L vanishes, namely $x_p > 0.2$.

Analogously to the ratio (1), measured previously in deep-inelastic scattering experiments [6], the ratio F_L/F_T was calculated. It is plotted in Fig. 4 together with the ratio F_L/F_{T+L} (see values in Table 2). A significant contribution from the longitudinal component is clearly seen in the region $x_p < 0.2$.

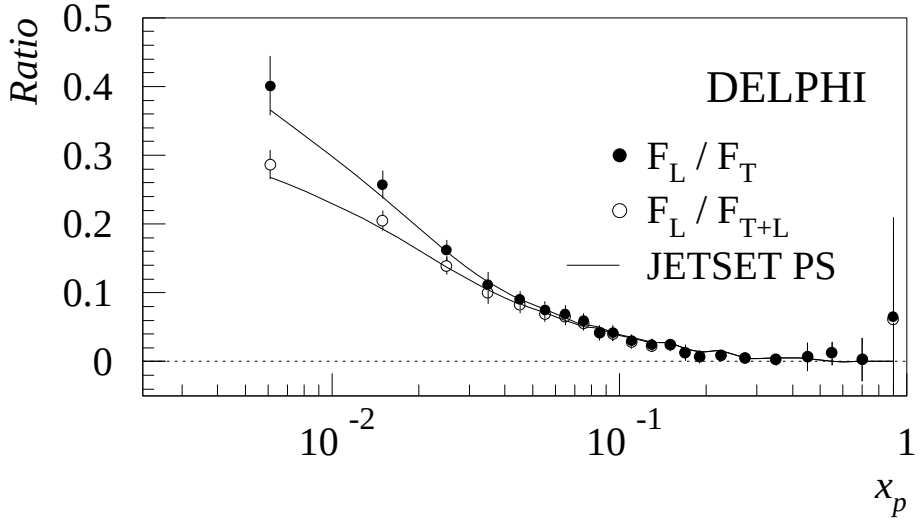

Figure 4: Ratio of the longitudinal to the transverse component of the fragmentation function and of the longitudinal component to the sum of both. Errors are both statistical and systematic.

3.2 Asymmetric fragmentation functions

The asymmetric component of the differential cross-section $F_A \equiv d\sigma_A^{ch}/dx_p$, see Eqs. (4) and (8), appears to be close to zero within errors, as expected, as can be seen from Fig. 5.

The charge asymmetric fragmentation function $\tilde{F}_A$, see Eq. (9), and the ratio $\tilde{F}_A/F_{T+L}$ are shown in Fig. 6. The corresponding JETSET 7.3 PS distributions are seen to agree qualitatively with the data. This charge asymmetric function $\tilde{F}_A$ is proportional to the vector coupling constants v_e and v_q which depend on the weak mixing angle [20]. The default value of $\sin^2\theta_W = 0.232$ was used in the JETSET model. However, studies performed with the JETSET PS model show that the sensitivity of $\tilde{F}_A$ and $\tilde{F}_A/F_{T+L}$ to $\sin^2\theta_W$ is rather weak. Furthermore, the lack of exact theoretical calculations for the dependence of $\tilde{F}_A(x_p)$ on the weak mixing angle in the full x_p interval also prevents extraction of a quantitative result on the value of $\sin^2\theta_W$.

Recently, theoretical leading order (LO), next-to leading order (NLO) and next-to-next-to-leading order (NNLO) QCD predictions of the shape of $\tilde{F}_A(x_p, M_Z)$ have been made [21]. Within the model assumptions used, the charge asymmetric fragmentation

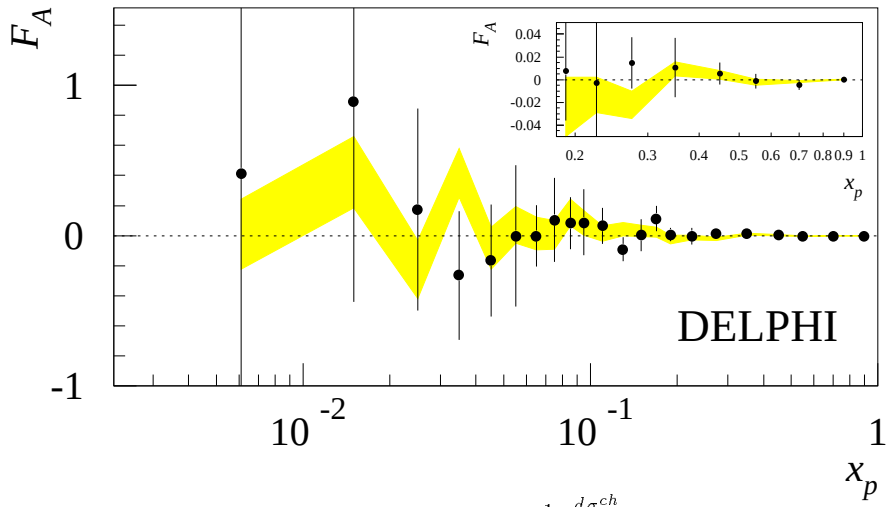

Figure 5: The asymmetric component $F_A \equiv \frac{1}{\sigma_{tot}} \frac{d\sigma_A^{ch}}{dx_p}$ of the fragmentation function for all charged hadrons, defined without reference to their charges. The combined statistical and systematic error is shown for each data point. This error is predominantly statistical for $x_p > 0.06$. The shaded band shows the asymmetric component obtained from the same analysis of the similar amount of JETSET generated events within one standard deviation. The inset shows the high x_p region with an expanded vertical scale.

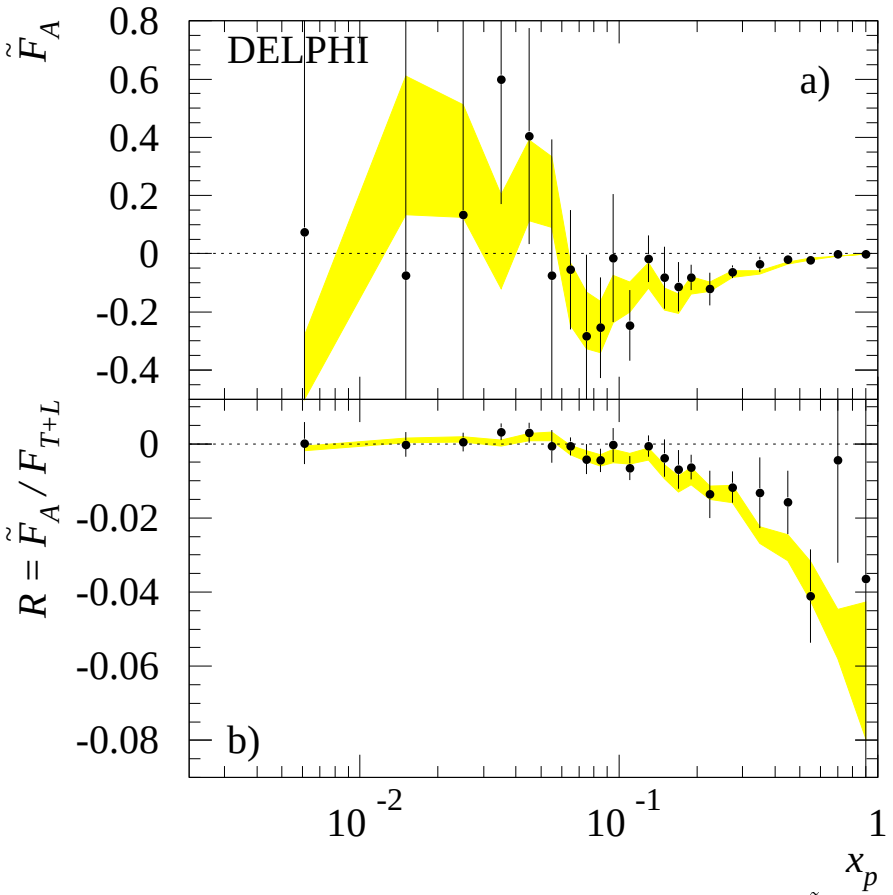

Figure 6: **a)** The 'charge asymmetric' fragmentation function $\tilde{F}_A$ and **b)** the ratio $\tilde{F}_A / F_{T+L}$ extracted from the DELPHI data. The combined statistical and systematic errors are shown. The shaded bands represent the same functions obtained from the analysis of the similar amount of JETSET generated events within one standard deviation.

function is expected to be negative in the whole x_p region; the first and second moments of $\tilde{F}_A$ calculated in the region $0.1 < x_p < 1$ are compared here with DELPHI results :

$$\begin{array}{lccc} & \text{NLO, NNLO} & \text{LO} & \text{DELPHI} \\ \int_{0.1}^{1} \tilde{F}_A dx_p = & -0.016 & -0.023 & -0.028 \pm 0.006(stat.+syst.) \\ \int_{0.1}^{1} \tilde{F}_A \frac{x_p}{2} dx_p = & -0.0020 & -0.0027 & -0.0036 \pm 0.0008(stat.+syst.) \end{array}$$

The present analysis gives values which are closer to the LO predictions than to the NLO and NNLO ones. The same discrepancy was observed in OPAL data [12] and, as discussed in [21], this can indicate that non-perturbative corrections to $\tilde{F}_A$ are essential.

4 Calculation of α_s

The cross-section components σ_L and σ_T in the inclusive annihilation process are infrared and collinear safe. The order α_s^2 and power corrections to σ_T and σ_L have been calculated recently [22–25]. In principle, this provides a possibility for a new measurement of α_s.

In the next-to-leading order of perturbative QCD, the full (charged plus neutral particles) longitudinal and transverse inclusive cross-sections, σ_L and σ_T, which are connected to the full fragmentation functions F_L and F_T analogously to equation (10), are expressed as [22] :

$$\frac{\sigma_L}{\sigma_{tot}} = 1 - \frac{\sigma_T}{\sigma_{tot}} = \frac{\alpha_s}{\pi} + \frac{\alpha_s^2}{\pi^2}(13.583 - N_f \cdot 1.028) \ , \tag{13}$$

where $N_f = 5$ is the number of active quark flavours.

While Eq. (13) refers to the full charged plus neutral particle cross-sections, in the present analysis only the charged particle cross-sections are measured. To perform the conversion from charged particles to charged plus neutral particles, the ratios of the inclusive charged to the full cross-sections, σ_L^{ch}/σ_L and σ_T^{ch}/σ_T, were studied in the JETSET 7.4 PS and HERWIG 5.9 models. As found previously by OPAL [12], they are approximately equal, with the values of the ratios found being $\sigma_T^{ch}/\sigma_T = 0.6308 \pm 0.0004$ and $\sigma_L^{ch}/\sigma_L = 0.624 \pm 0.005$ in JETSET, and $\sigma_T^{ch}/\sigma_T = 0.6019 \pm 0.0005$ and $\sigma_L^{ch}/\sigma_L = 0.603 \pm 0.007$ in HERWIG.

Assuming this equality gives the following values for the ratios of the full inclusive cross-sections :

$$\begin{aligned} \frac{\sigma_T}{\sigma_{tot}} &= \frac{\sigma_T^{ch}}{\sigma_L^{ch} + \sigma_T^{ch}} = 0.949 \pm 0.001(stat.) \pm 0.007(syst.), \\ \frac{\sigma_L}{\sigma_{tot}} &= \frac{\sigma_L^{ch}}{\sigma_L^{ch} + \sigma_T^{ch}} = 0.051 \pm 0.001(stat.) \pm 0.007(syst.), \end{aligned} \tag{14}$$

where the systematic uncertainties quoted correspond to those on $\sigma_T^{ch}/\sigma_{tot}$ and $\sigma_L^{ch}/\sigma_{tot}$ (see Section 5). Small differences of about 1% between the ratios σ_L^{ch}/σ_L and σ_T^{ch}/σ_T would not lead to significant changes in σ_T/σ_{tot} or σ_L/σ_{tot}.

Substituting the value of σ_L/σ_{tot} into (13) gives the strong interaction coupling constant,

$$\alpha_s^{NLO}(M_Z) = 0.120 \pm 0.002(stat.) \pm 0.013(syst.) \ . \tag{15}$$

In the order α_s^2 calculations [22], the ratios σ_L/σ_{tot} and σ_T/σ_{tot} depend on the mass factorisation scale μ and renormalization scale R. Equation (13) and the value of α_s in (15) correspond to $\mu = R = M_Z$. The dependence of α_s on the factorisation and renormalization scales (assuming $\mu = R$) is shown in Fig. 7. Between $\mu = 2Q$ and $\mu = Q/2$, the value of α_s changes by about 12%. This gives an additional error of ± 0.007.

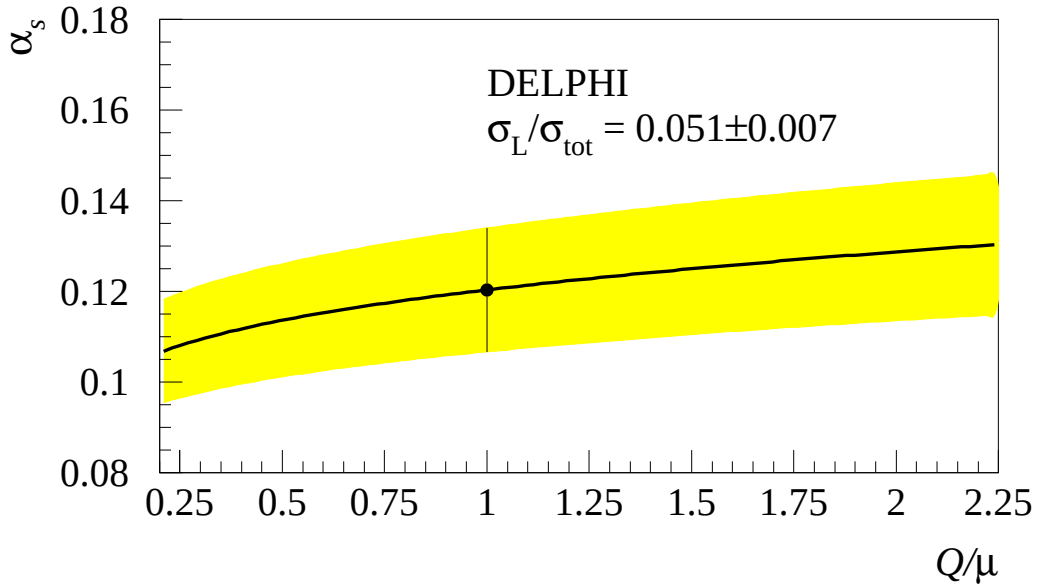

Figure 7: Dependence of the strong coupling constant α_s on the factorisation and renormalization scales ($\mu = R$). The shaded region shows the $\pm 1\sigma$ error band. The point indicates the α_s value obtained in this work for $\mu = Q$.

Non-perturbative corrections to the value of $\delta\sigma_L/\sigma_{tot}$ have also been calculated recently [23,24]. They appear to be comparable with the next-to-leading order contributions. These corrections, which are also known as power corrections, were obtained by different methods, each of which led to a similar $\propto 1/Q$ behaviour. At LEP1 energies, the value of the power corrections calculated in [23] under the assumption of an infrared-regular effective behaviour of α_s was given as $(\delta\sigma_L/\sigma_{tot})^{POW} = 0.010 \pm 0.001$. A similar estimate of the power corrections to the longitudinal and transverse cross-sections was also obtained in [25], based on the assumption of ultraviolet dominance of higher-twist matrix elements. Studies performed with the JETSET 7.4 PS suggest corrections of the same magnitude.

Accounting for this estimate of the non-perturbative power corrections changes the α_s value of (15) to

$$\alpha_s^{NLO+POW}(M_Z) = 0.101 \pm 0.002(stat.) \pm 0.013(syst.) \pm 0.007(scale), \qquad (16)$$

where the scale uncertainty again comes from varying the renormalisation scale in the range $0.5 < Q/\mu < 2$ (see Fig. 7).

5 Studies of systematic effects

Several sources of systematic uncertainties were considered in the estimates quoted above. A study of the systematic deviations of the fragmentation functions caused by

the detector features and selection criteria was described in [5]. Analogous studies are performed here to estimate the systematics on the components of the fragmentation function and other measured variables, like the charged particle multiplicity and the cross-section components. The total systematic errors on F_T and F_L together with the three main contributions are shown as a function of x_p in Table 3. Table 4 shows the systematic error estimates for $\sigma_T^{ch}/\sigma_{tot}$, $\sigma_L^{ch}/\sigma_{tot}$ and $\langle n^{ch} \rangle$.

Firstly, changes of the measured values under variations of the track and event selection criteria described in Section 2 were considered. The most significant changes arose from varying the impact parameter cut, reflecting the influence of short-living mesons and baryons and also of secondary interactions in the detector material, which distort the reconstructed impact parameter distributions and the inclusive spectra. Varying the cut on the polar angle of the event sphericity axis also led to significant changes, since it affected the angular distribution of the hadrons. Varying the cut on the polar angles of the tracks also gave deviations which exceeded the statistical errors. Changing the selection on the minimum particle momentum led to significant deviations in the very first bin, $0 < x_p < 0.01$. Varying other cuts gave less significant changes, not exceeding the corresponding statistical uncertainties.

To study the systematics related to the angular range limitation, the range analysed was varied from $|\cos\theta| < 0.5$ up to $|\cos\theta| < 0.9$, and the average deviation of the resulting values was considered as a systematic uncertainty. Changing the number of points involved in the analysis obviously affects the statistics. To separate out this statistical contribution to the observed deviations, the same analysis was performed on distributions generated by the JETSET 7.3 PS model with a similar number of events. The systematics were estimated by subtracting in quadrature the deviations obtained with the JETSET samples from those obtained with the DELPHI data.

Another source of systematic uncertainty is the angular region around $\cos\theta \approx 0$, where the charged particle reconstruction efficiency is relatively poor (see Fig. 1), due to the effect of the mid-plane of the TPC [14]. To study the influence of this effect, the analysis was repeated with the points between $-0.1 < \cos\theta < 0.1$ replaced by the values of the fitting function (12).

As mentioned above, the weighting and fitting methods gave slightly different results. Studies using generated JETSET PS events showed that the values of F_T from the fitting procedure are systematically higher, and those of F_L systematically lower, than those obtained by weighting. The difference does not exceed the statistical errors for F_T and F_L; it is significant only for $\sigma_L^{ch}/\sigma_{tot}$, where it amounts to 2.5%. The results of the weighting method are closer to those of the JETSET PS generator model than those of the fitting method.

In the determination of the components of the cross-section, proper knowledge of the mean x_p value in each histogram bin plays an important role. To estimate possible uncertainties connected to the association of x_p value with each bin, $\sigma_T^{ch}/\sigma_{tot}$ and $\sigma_L^{ch}/\sigma_{tot}$ were alternatively evaluated as

$$\frac{\sigma_P^{ch}}{\sigma_{tot}} = \frac{1}{\sigma_{tot}} \int_{-v}^{+v} W_P \, d\cos\theta \int_0^1 \frac{x_p}{2} \frac{d^2\sigma^{ch}}{dx_p d\cos\theta} dx_p \ , \tag{17}$$

where $P = T, L$ and integration over dx_p was performed using the actual x_p value for each measured track, instead of histogramming. The cross-sections obtained with this method differed by about 0.2% for transverse and 0.6% for longitudinal components.

Another source of systematics, connected to the mean charged multiplicity, is the fact that the JETSET event generator produces slightly different numbers of K_S^0 and

Λ than are measured experimentally [17]. Studies of the influence of this effect showed that varying the average K^0_S multiplicity by $\pm 5\%$ leads to a change in measured $\langle n^{ch} \rangle$ of ± 0.02. Varying the mean Λ multiplicity did not lead to a significant change in $\langle n^{ch} \rangle$.

Discrepancy between the data collected during 1992 and 1993 data taking periods also contributes to the total systematic uncertainty. However, it exceeds the statistical error only in the region of $x_p < 0.06$.

The quadratic sum of all the above mentioned errors is represented in Tables 3 and 4 as the total systematic uncertainty.

While in perturbation theory the Bjorken x ($x = x_E$) variable is used for fragmentation function calculations, in e^+e^- annihilation it is usually replaced by the x_p variable. Tests using the JETSET generator showed that for F_T and F_L the substitution of x_p with x_E affects only the region $x_p < 0.02$, which is due to mass effects. For cross-sections it causes deviations of approximately 0.3% in the transverse and 2% in the longitudinal component.

6 b and uds enriched event samples

Samples of events originating from quarks of different flavours were selected using the lifetime tag variable P_H [15], defined as the probability for the hypothesis that all the charged particle tracks in a given hemisphere with respect to the thrust axis came from a single primary vertex. Since hadrons containing b quarks have a high charged particle decay multiplicity and a long lifetime ($\approx$ 1.55 ps), and are produced with a high momentum at LEP, this single-vertex probability is small for $Z^0 \to b\overline{b}$ events. The selection was done assuming, according to the simulation, that requiring $P_H < 10^{-3}$ selects $b\overline{b}$ events with purity $\approx 94\%$ and efficiency $\approx 16\%$, and requiring $P_H > 0.3$ selects light quark events with purity $\approx 73\%$ and efficiency $\approx 72\%$. The particles to be analysed were then taken from the opposite hemisphere.

The selected samples consisted of about 42,000 b events and 610,000 uds events. The contamination by heavy flavours in the uds events was estimated to be $\approx$ 11% from bottom and $\approx$ 16% from charm quarks.

As mentioned in Section 2, all experimental distributions have been multiplied by correction factors. These were calculated using (3), with the "true" spectra taken from pure generated b or uds events and the "reconstructed" ones obtained using the DELSIM detector simulation [15] and applying the lifetime tagging procedure to the fully simulated events.

The procedure described in Sect. 3 for separating the longitudinal and transverse components of the fragmentation function was applied to the corrected b and uds event samples. The components of the fragmentation functions for different quark flavours were defined as

$$F_P^q \equiv \frac{1}{\sigma_{tot}^q} \frac{d\sigma_P^q}{dx_p} \,, \tag{18}$$

where $P = T, L$ and $q = uds, b$. The results are shown in Fig. 8 and Table 5.

The charged particle multiplicities in b and uds events were obtained by integrating the fragmentation functions as described in Section 3.1. These too are presented in Table 5, and are in qualitative agreement with the overall multiplicity (11). The charged multiplicity observed in b events is in good agreement with previous DELPHI results [26].

The main difference between the b and uds spectra comes from the transverse component of the cross-section, which is softer for the b quark sample. There is no significant

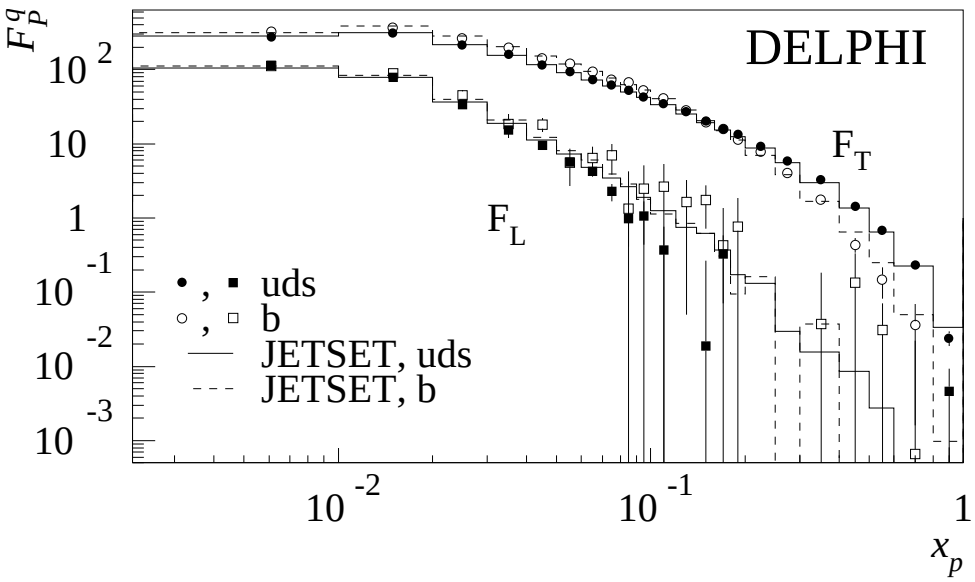

Figure 8: Transverse and longitudinal components of the fragmentation functions of different quark flavours. Errors include both statistical and systematic ones. For b-tagged events, the systematics do not exceed the statistical uncertainties. For light quark events, the systematics dominate mainly in the region $0 < x_p < 0.12$, where they amount to $\pm 1.5\%$ for F_T and about $\pm 10\%$ for F_L.

difference between the longitudinal fragmentation functions F_L^{uds} and F_L^b. The fragmentation function components obtained from the analysis of the JETSET 7.3 PS generated events have the same behaviour as the data.

Studies of systematic uncertainties were performed as described in Section 5. For b-tagged events, the systematics do not exceed the statistical uncertainties. For light quark events, the systematics dominate mainly in the region $0 < x_p < 0.12$, where they amount to $\pm 1.5\%$ for F_T and about $\pm 10\%$ for F_L.

7 Gluon fragmentation function

According to perturbative QCD, the longitudinal component of the fragmentation function is equal to zero in leading order (LO) of α_s [7,27,28], and is given in next-to-leading order by [8,9] :

$$\begin{aligned} F_L(x_p) &= \frac{\alpha_s^{LO}(M_Z)}{2\pi} C_F \int_{x_p}^{1} \frac{F_T(z)}{z} dz \\ &+ \frac{2\alpha_s^{LO}(M_Z)}{\pi} C_F \int_{x_p}^{1} \left(\frac{z}{x_p} - 1 \right) D_g(z) \frac{dz}{z} + \mathcal{O}(\alpha_s^2) \ , \end{aligned} \tag{19}$$

where the colour factor $C_F = 4/3$ and $D_g(z)$ is a function which describes fragmentation of gluons into hadrons, given in leading order. This formula (19) contains the leading order expression for α_s^{LO} :

$$\alpha_s^{LO}(Q) = \frac{4\pi}{\beta_0 \ln(\frac{Q^2}{\Lambda_{LO}^2})} \ , \tag{20}$$

where $\beta_0 = 11 - \frac{2}{3}N_f$, N_f is the number of active quark flavours, Q is the centre-of-mass energy, and $\Lambda_{LO} \equiv \Lambda_{LO}^{(N_f)}$ is the QCD scale parameter. In what follows, α_s is everywhere given for $N_f = 5$. Strictly speaking, expression (19) is not valid in the region where F_L approaches zero, thus it can be used only as an approximation.

Applying the perturbative formula (19) implies knowledge of the α_s^{LO} value consistent with the perturbation analysis. However, experimental results are presented mostly in terms of the next-to-leading order value of α_s only, thus a special analysis should be done to extract the value of α_s^{LO}.

OPAL [12] used for this purpose the approximate ratio $\sigma_L/\sigma_T = \alpha_s^{LO}/\pi$, which can contain higher order and non-perturbative hadronization effects. This method gave a value of $\alpha_s^{LO}(M_Z) = 0.190$ for OPAL data and $\alpha_s^{LO}(M_Z) = 0.171$ for this analysis.

Alternatively, results from deep inelastic scattering experiments at high Q^2 can be used, since perturbation theory is known to be applicable there. To determine the leading order value of $\alpha_s^{LO}(M_Z)$, the QCD scale parameter $\Lambda_{LO}^{(4)}$, found by the BCDMS collaboration [29] was recalculated to $\alpha_s^{LO}(M_Z) = 0.126 \pm 0.006$. A recent analysis of LEP and lower energy e^+e^- annihilation data [30] gave $\alpha_s^{LO}(M_Z) \approx 0.122$.

A third approach is to treat α_s^{LO} as a free parameter of a fit to the measured function F_L using (19) neglecting $\mathcal{O}(\alpha_s^2)$ terms, similar to the ALEPH analysis [13].

The gluon fragmentation function $D_g(x_p)$ can be parameterized by the form [12,13]

$$D_g(x_p) = P_1 \cdot x_p^{P_2}(1 - x_p)^{P_3} e^{-P_4 \ln^2 x_p} \ , \tag{21}$$

where the P_i are free parameters of the fitting procedure. This parametrization is purely phenomenological. The form (21) implies also a strong correlation between the parameters P_i, suggesting that any set of values which describes the D_g may not be unique.

The fit was performed using the measured transverse and longitudinal fragmentation functions F_L and F_T given in Table 1. The x_p interval $0.01 < x_p < 0.6$ was used, in order to stay in the region where F_L is well measured and to avoid the small x_p region, where systematic uncertainties and non-perturbative effects are large.

The strong correlation between the parameters P_i and between the values of α_s^{LO} and P_i, as well as the approximate nature of the fit due to the omission of $\mathcal{O}(\alpha_s^2)$ terms, suggest that special investigation of the uncertainty in D_g is required. To estimate it, the fit was performed in two different conditions, either with a predefined value of $\alpha_s^{LO} = 0.126$ or allowing α_s^{LO} to vary freely. Also, two different data samples were used: a) the F_L and F_T values measured in all hadronic events quoted in Table 1, b) the F_L and F_T values measured in heavy-quark and light-quark tagged events quoted in Table 5 and those measured in the remaining untagged events. The fragmentation functions of the tagged quarks and of the remaining quark mixture were fitted simultaneously, assuming the same shape for the gluon fragmentation function. Parameters evaluated with α_s^{LO} either fixed at the value 0.126 or being a free parameter are shown in Table 6.

The gluon fragmentation function $D_g(x_p)$ corresponding to the parameter values obtained by fitting the F_L and F_T values measured for the natural flavour mix events (see Table 1) with α_s^{LO} free is plotted in Fig. 9 in the x_p interval used in the fit. Similar fits done by the OPAL [12] and ALEPH [13] collaborations are also shown, together with the result of a similar fit to the JETSET PS generated events. In spite of having different sets of parameters in (21) (see Table 6 and references [12,13]), D_g functions obtained by OPAL, ALEPH and DELPHI are in satisfactory agreement. The results obtained also exhibit a low sensitivity to α_s^{LO}, which stems from the strong correlation between α_s^{LO} and D_g and from the semi-empirical nature of the method.

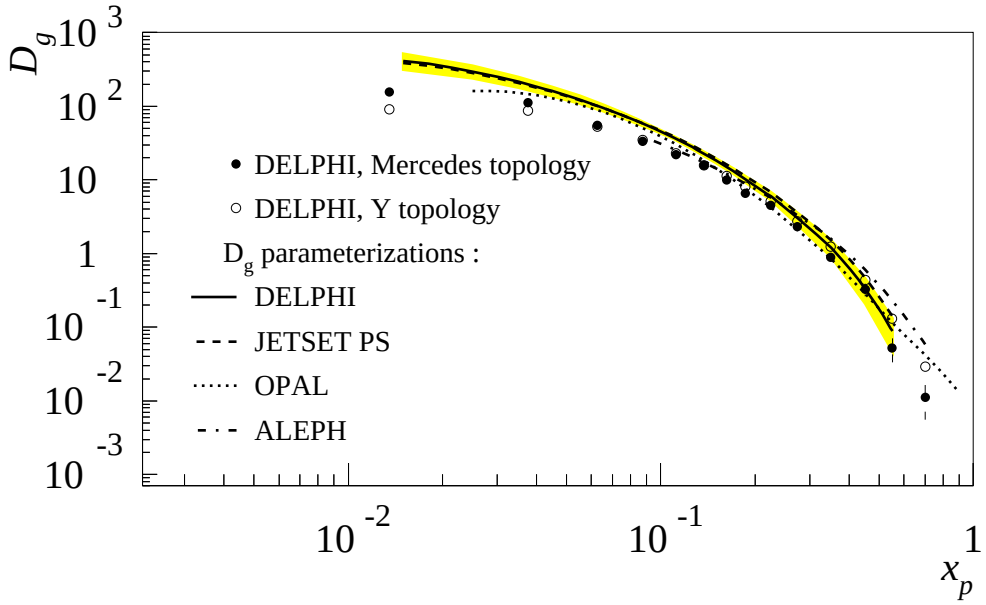

Figure 9: Gluon fragmentation functions $D_g(x_p)$ as obtained from the DELPHI data (full curve, with shaded band showing the uncertainty in D_g) using a fit with the parametrization (21), and by OPAL (dotted curve) and ALEPH (dot-dashed curve) with the same parametrization, compared with a similar fit to distributions generated with the JETSET PS model (dashed curve) and with charged particle spectra from gluon jets in events of different topologies [31] (open and closed circles).

Recently, DELPHI presented measurements of the gluon fragmentation function using a procedure for separating quark and gluon jets in three-jet events [31]. Fig. 9 also compares the gluon fragmentation functions $D_g(x_p)$ with the inclusive particle distributions in gluon jets obtained in this way. The two measurements are complementary. They are in reasonable agreement in the region of $x_p > 0.2$, but there is a systematic difference at small x_p. The method based on fitting F_L and F_T with equation (19) has some limitations, because that equation is valid only in the next-to-leading order of perturbative QCD. However, it is independent of the jet definition and therefore is potentially more reliable in the region of small x_p, where the assignment of particles to jets is arbitrary. In addition, the gluon fragmentation functions obtained with these two methods might have different behaviours due to the effect of Q^2 dependence, because the selected gluon samples have different average energies.

Fig. 10 compares the gluon fragmentation function $D_g(x_p)$ with the transverse fragmentation function $F_T(x_p)$, which can be considered as a quark fragmentation function at large values of x_p, where $F_L(x_p)$ can be neglected. There is a clear indication that the gluon spectrum is softer, as qualitatively predicted by QCD.

8 Summary

Data collected by DELPHI in 1992 and 1993 have been used to measure the inclusive charged hadron cross-section in the full available x_p and polar angle θ intervals. Using the weighting functions method, the transverse F_T, longitudinal F_L and charge asymmetry $\tilde{F}_A$ fragmentation functions were evaluated from the double differential charged hadron cross-section $d^2\sigma^{ch}/dx_p d\cos\theta$. Available statistics of more than one million events allow precise measurement of the longitudinal fragmentation function, which serves as an important

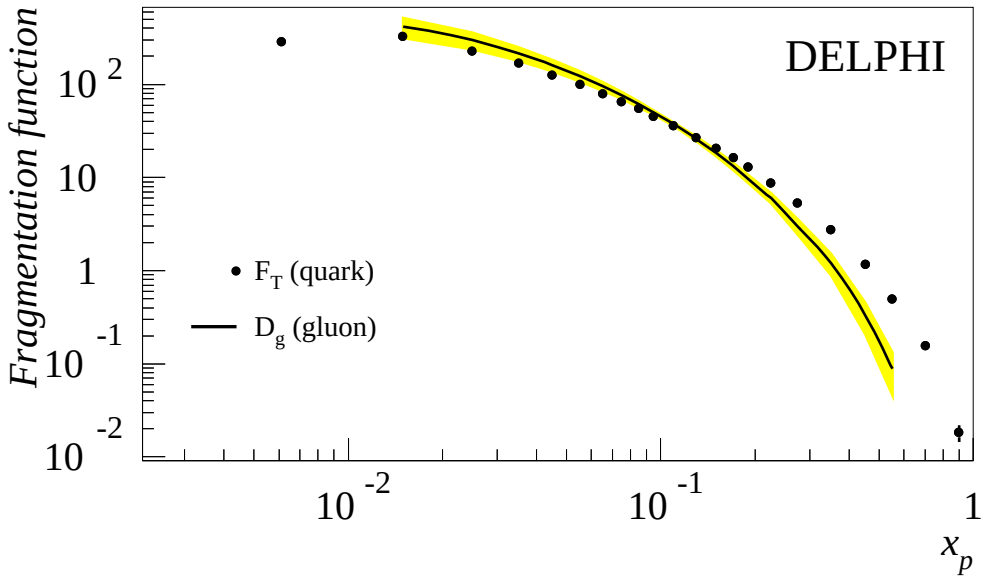

Figure 10: Comparison of the gluon fragmentation function $D_g(x_p)$ with the transverse fragmentation function $F_T(x_p)$ (as in Figure 2). The shaded band shows the range of D_g deviations.

test of QCD. Confirming qualitative theoretical predictions, F_L was found to be non-zero in the region of $x_p < 0.2$ and vanishing at higher x_p.

The transverse σ_T/σ_{tot} and longitudinal σ_L/σ_{tot} fractions of the charged hadron cross-section, defined as the second moments of the corresponding fragmentation functions, were inferred from the data. The value of $\sigma_L/\sigma_{tot} = 0.051 \pm 0.007$ obtained was used to calculate the strong coupling constant $\alpha_s(M_Z)$ to the next-to-leading order of perturbative QCD, giving $\alpha_s^{NLO}(M_Z) = 0.120 \pm 0.013$. Inclusion of non-perturbative power corrections led to the value of $\alpha_s^{NLO+POW}(M_Z) = 0.101 \pm 0.013$.

The measured functions F_T and F_L were used to estimate the mean charged multiplicity, which was found to be $\langle n^{ch} \rangle = 21.21 \pm 0.20$. This value takes into account particle reconstruction inefficiencies in the forward regions of the detector through the weighting functions.

The charge asymmetry fragmentation function $\tilde{F}_A$ is connected to the electroweak theory parameter $\sin^2\theta_W$. Measured data are consistent with the value $\sin^2\theta_W = 0.232$ which was used as an input parameter for JETSET.

Using the lifetime tagging procedure, F_T and F_L were measured from b and uds enriched event samples. Performing simultaneous fit of measured fragmentation functions, the parametrization of the gluon fragmentation function D_g was made. Comparison of D_g to F_T, which is considered as the quark fragmentation function to the leading order of QCD, confirms qualitative QCD prediction, that the gluon fragmentation function is softer than the quark one.

9 Acknowledgements

We are greatly indebted to our technical collaborators and to the funding agencies for their support in building and operating the DELPHI detector, and to the members of the CERN-SL Division for the excellent performance of the LEP collider.

References

[1] V. N. Gribov and L. N. Lipatov, Sov. J. Nucl. Phys. **15** (1972) 78;
G. Altarelli, G. Parisi, Nucl. Phys. **B126** (1977) 298;
Yu. L. Dokshitser, Sov. Phys. JETP **46** (1977) 641.

[2] K. Kato, K. Kitani, T. Munehisa, H. Okada and Y. Shimizu, Phys. Rev. Lett. **50** (1983) 389;
K. Kato, T. Munehisa, H. Okada and Y. Shimizu, Prog. Theor. Phys. **70** (1983) 840.

[3] E. P. Velicheva, S. P. Kurlovich, N. B. Skachkov, "New DELPHI Data on Inclusive $e^+e^- \to h + X$ Process and Check of QCD Predictions for Scaling Violations in Fragmentation Functions", Dubna JINR-1(47)-91-5 (1991);
N. B. Skachkov, "On the Determination of α_s from QCD Analysis of the Scaling Violation in the Fragmentation Functions of the Process $e^+e^- \to h + X$ Studied by DELPHI, TASSO, and Other Collaborations", Dubna JINR-E2-95-189 (1995).

[4] DELPHI Coll., P. Abreu et al., Phys. Lett. **B398** (1997) 194.

[5] DELPHI Coll., P. Abreu et al., Phys. Lett. **B311** (1993) 408.

[6] EMC Coll., J.J. Aubert et al., Phys.Lett. **B121** (1983) 87;
BCDMS Coll., A. C. Benvenuti et al., Phys. Lett. **B237** (1990) 592;
E140X Coll., L. H. Tao et al., Z. Phys. **C70** (1996) 387.

[7] A. Buras, Rev. Mod. Phys. **52** (1980) 199.

[8] G. Altarelli et al., Nucl. Phys. **B160** (1979) 301.

[9] G. Altarelli et al., Phys. Rep. **81 N1** (1982) 1.

[10] TASSO Coll., R. Brandelik et al., Phys. Lett. **B114** (1982) 65.

[11] N. B. Skachkov and L. G. Tkatchev, "On the Determination of the Longitudinal Component of the Fragmentation Function of the Process $e^+e^- \to h + X$", DELPHI Note 92-112 PHYS 218, contrib. to ICHEP Conf., Dallas (1992), unpublished.

[12] OPAL Coll., R. Akers et al., Z. Phys. **C68** (1995) 203.

[13] ALEPH Coll., D. Buskulic et al., Phys. Lett. **B357** (1995) 487.

[14] DELPHI Coll., P. Aarnio et al., Nucl. Instr. & Meth. **A 303** (1991) 233.

[15] DELPHI Coll., P. Abreu et al., Nucl. Instr. & Meth. **A378** (1996) 57.

[16] T. Sjöstrand, Comp. Phys. Comm. **28** (1983) 229;
T. Sjöstrand, "PYTHIA 5.6 and JETSET 7.3", CERN-TH.6488/92 (1992).

[17] DELPHI Coll., P. Abreu et al., Z. Phys. **C73** (1996) 11.

[18] P. Nason, B. R. Webber, Nucl. Phys. **B421** (1994) 473.

[19] PDG, R.M. Barnett et al., Phys. Rev. **D54** (1996) 1.

[20] P. Nason, B. R. Webber, Phys. Lett. **B332** (1994) 405.

[21] P. J. Rijken, W. L. van Neerven, Phys. Lett. **B392** (1997) 207.

[22] P. J. Rijken, W. L. van Neerven, Phys. Lett. **B386** (1996) 422.

[23] Yu. L. Dokshitser, B. R. Webber, Phys. Lett. **B352** (1995) 451.

[24] M. Dasgupta, B. R. Webber, Nucl. Phys. **B484** (1997) 247.

[25] M. Beneke, V. M. Braun, L. Magnea, Nucl. Phys. **B497** (1997) 297.

[26] DELPHI Coll., P. Abreu et al., Phys. Lett. **B347** (1995) 447.

[27] G. Curci, W. Furmanski, R. Petronzio, Nucl. Phys. **B175** (1980) 27.

[28] E. G. Floratos, C. Kounnas, R. Lacaze, Nucl. Phys. **B192** (1981) 417.

[29] BCDMS Coll., A .Benvenuti et al., Phys. Lett. **B223** (1989) 490.

[30] J. Binnewies, B. A. Kniehl, G. Kramer, Phys. Rev. **D52** (1995) 4947.

[31] DELPHI Coll., P. Abreu et al., Zeit. Phys. **C70** (1996) 179.

x_p range	$F_T(x_p)$	$F_L(x_p)$	$\tilde{F}_A(x_p)$	$F_{T+L}(x_p)$
$0.00-0.01$	$291.6 \pm 0.9 \pm 13.0$	$117.0 \pm 0.7 \pm 7.5$	$0.07 \pm 0.48 \pm 2.28$	$408.6 \pm 0.4 \pm 8.6$
$0.01-0.02$	$326.9 \pm 0.6 \pm 6.1$	$84.2 \pm 0.4 \pm 5.5$	$-0.08 \pm 0.30 \pm 1.30$	$411.1 \pm 0.3 \pm 3.1$
$0.02-0.03$	$229.4 \pm 0.5 \pm 3.4$	$37.1 \pm 0.4 \pm 3.2$	$0.13 \pm 0.25 \pm 0.62$	$266.4 \pm 0.2 \pm 2.4$
$0.03-0.04$	$167.2 \pm 0.4 \pm 3.8$	$18.5 \pm 0.3 \pm 2.9$	$0.60 \pm 0.21 \pm 0.38$	$185.7 \pm 0.2 \pm 2.2$
$0.04-0.05$	$126.4 \pm 0.4 \pm 1.8$	$11.3 \pm 0.3 \pm 1.6$	$0.41 \pm 0.18 \pm 0.33$	$137.7 \pm 0.1 \pm 1.4$
$0.05-0.06$	$98.4 \pm 0.3 \pm 1.6$	$7.4 \pm 0.2 \pm 1.2$	$-0.08 \pm 0.16 \pm 0.44$	$105.7 \pm 0.1 \pm 1.2$
$0.06-0.07$	$78.7 \pm 0.3 \pm 1.4$	$5.5 \pm 0.2 \pm 0.9$	$-0.05 \pm 0.14 \pm 0.15$	$84.2 \pm 0.1 \pm 1.0$
$0.07-0.08$	$64.5 \pm 0.3 \pm 1.0$	$3.8 \pm 0.2 \pm 0.7$	$-0.28 \pm 0.13 \pm 0.25$	$68.3 \pm 0.1 \pm 0.8$
$0.08-0.09$	$54.4 \pm 0.2 \pm 0.8$	$2.3 \pm 0.2 \pm 0.5$	$-0.25 \pm 0.12 \pm 0.13$	$56.70 \pm 0.10 \pm 0.69$
$0.09-0.10$	$45.6 \pm 0.2 \pm 0.8$	$1.9 \pm 0.2 \pm 0.5$	$-0.02 \pm 0.11 \pm 0.19$	$47.52 \pm 0.09 \pm 0.59$
$0.10-0.12$	$36.2 \pm 0.1 \pm 0.6$	$1.1 \pm 0.1 \pm 0.3$	$-0.25 \pm 0.07 \pm 0.10$	$37.31 \pm 0.06 \pm 0.46$
$0.12-0.14$	$27.1 \pm 0.1 \pm 0.4$	$0.64 \pm 0.08 \pm 0.25$	$-0.02 \pm 0.06 \pm 0.06$	$27.71 \pm 0.05 \pm 0.37$
$0.14-0.16$	$20.6 \pm 0.1 \pm 0.3$	$0.50 \pm 0.07 \pm 0.15$	$-0.08 \pm 0.05 \pm 0.09$	$21.12 \pm 0.04 \pm 0.26$
$0.16-0.18$	$16.27 \pm 0.09 \pm 0.28$	$0.21 \pm 0.07 \pm 0.17$	$-0.11 \pm 0.05 \pm 0.07$	$16.38 \pm 0.04 \pm 0.23$
$0.18-0.20$	$12.88 \pm 0.08 \pm 0.20$	$0.09 \pm 0.06 \pm 0.10$	$-0.08 \pm 0.04 \pm 0.02$	$12.97 \pm 0.03 \pm 0.17$
$0.20-0.25$	$8.79 \pm 0.04 \pm 0.13$	$0.08 \pm 0.03 \pm 0.05$	$-0.12 \pm 0.02 \pm 0.05$	$8.87 \pm 0.02 \pm 0.11$
$0.25-0.30$	$5.29 \pm 0.03 \pm 0.08$	$0.03 \pm 0.02 \pm 0.03$	$-0.06 \pm 0.02 \pm 0.02$	$5.31 \pm 0.01 \pm 0.07$
$0.30-0.40$	$2.73 \pm 0.02 \pm 0.07$	$0.007 \pm 0.012 \pm 0.020$	$-0.036 \pm 0.009 \pm 0.025$	$2.734 \pm 0.007 \pm 0.057$
$0.40-0.50$	$1.16 \pm 0.01 \pm 0.04$	$0.008 \pm 0.008 \pm 0.022$	$-0.018 \pm 0.006 \pm 0.008$	$1.167 \pm 0.005 \pm 0.019$
$0.50-0.60$	$0.502 \pm 0.007 \pm 0.010$	$0.006 \pm 0.005 \pm 0.007$	$-0.021 \pm 0.004 \pm 0.005$	$0.508 \pm 0.003 \pm 0.008$
$0.60-0.80$	$0.155 \pm 0.003 \pm 0.007$	$0.0004 \pm 0.0021 \pm 0.0043$	$-0.0007 \pm 0.0015 \pm 0.0040$	$0.155 \pm 0.001 \pm 0.008$
$0.80-1.00$	$0.018 \pm 0.001 \pm 0.003$	$0.0012 \pm 0.0007 \pm 0.0020$	$-0.0007 \pm 0.0005 \pm 0.0017$	$0.0193 \pm 0.0004 \pm 0.0023$
$\sigma_P^{ch}/\sigma_{tot}$	$0.5788 \pm 0.0007 \pm 0.0068$	$0.0309 \pm 0.0005 \pm 0.0042$	—	$0.6097 \pm 0.0003 \pm 0.0066$

Table 1: Transverse $F_T(x_p)$, longitudinal $F_L(x_p)$ and asymmetric $\tilde{F}_A(x_p)$ components of the fragmentation function, and the summed function $F_{T+L}(x_p)$, measured using the weighting method. The $\sigma_P^{ch}/\sigma_{tot}$ $(P = T, L, T+L)$ are the corresponding fractions of the charged particle cross-section. The first error is statistical and the second one is systematic. The function $F_{T+L}(x_p)$ was evaluated from the double-differential cross-section by applying the weight $(W_T + W_L)$ and integrating over the angular range $|\cos\theta| < 0.8$. The smallness of the errors on $F_{T+L}(x_p)$ reflects the anti-correlation between the errors on F_T and F_L.

x_p range	F_L/F_T	F_L/F_{T+L}
$0.00 - 0.01$	$0.401 \pm 0.004 \pm 0.043$	$0.286 \pm 0.002 \pm 0.021$
$0.01 - 0.02$	$0.258 \pm 0.002 \pm 0.021$	$0.205 \pm 0.001 \pm 0.014$
$0.02 - 0.03$	$0.162 \pm 0.002 \pm 0.016$	$0.139 \pm 0.001 \pm 0.013$
$0.03 - 0.04$	$0.111 \pm 0.002 \pm 0.019$	$0.100 \pm 0.002 \pm 0.016$
$0.04 - 0.05$	$0.090 \pm 0.002 \pm 0.013$	$0.082 \pm 0.002 \pm 0.012$
$0.05 - 0.06$	$0.075 \pm 0.003 \pm 0.012$	$0.070 \pm 0.002 \pm 0.011$
$0.06 - 0.07$	$0.069 \pm 0.003 \pm 0.013$	$0.065 \pm 0.002 \pm 0.012$
$0.07 - 0.08$	$0.059 \pm 0.003 \pm 0.011$	$0.056 \pm 0.003 \pm 0.010$
$0.08 - 0.09$	$0.043 \pm 0.003 \pm 0.010$	$0.041 \pm 0.003 \pm 0.010$
$0.09 - 0.10$	$0.042 \pm 0.003 \pm 0.011$	$0.040 \pm 0.003 \pm 0.010$
$0.10 - 0.12$	$0.030 \pm 0.003 \pm 0.009$	$0.029 \pm 0.003 \pm 0.009$
$0.12 - 0.14$	$0.024 \pm 0.003 \pm 0.009$	$0.023 \pm 0.003 \pm 0.009$
$0.14 - 0.16$	$0.024 \pm 0.004 \pm 0.007$	$0.024 \pm 0.004 \pm 0.008$
$0.16 - 0.18$	$0.013 \pm 0.004 \pm 0.011$	$0.013 \pm 0.004 \pm 0.010$
$0.18 - 0.20$	$0.007 \pm 0.005 \pm 0.008$	$0.007 \pm 0.005 \pm 0.008$
$0.20 - 0.25$	$0.009 \pm 0.004 \pm 0.006$	$0.009 \pm 0.004 \pm 0.006$
$0.25 - 0.30$	$0.005 \pm 0.005 \pm 0.005$	$0.005 \pm 0.005 \pm 0.006$
$0.30 - 0.40$	$0.003 \pm 0.004 \pm 0.007$	$0.003 \pm 0.005 \pm 0.007$
$0.40 - 0.50$	$0.007 \pm 0.007 \pm 0.019$	$0.007 \pm 0.007 \pm 0.019$
$0.50 - 0.60$	$0.012 \pm 0.011 \pm 0.014$	$0.012 \pm 0.010 \pm 0.013$
$0.60 - 0.80$	$0.003 \pm 0.014 \pm 0.029$	$0.003 \pm 0.014 \pm 0.028$
$0.80 - 1.00$	$0.065 \pm 0.044 \pm 0.139$	$0.061 \pm 0.039 \pm 0.119$

Table 2: Ratio of the longitudinal to the transverse component of the fragmentation function and to the sum of the longitudinal and transverse components. Statistical and systematic errors are shown. The systematic uncertainties are correlated between x_p bins.

x_p range	Track/event selection		Angular range		Region of $\lvert\cos\theta\rvert \approx 0$		Total	
	ΔF_T	ΔF_L	ΔF_T	ΔF_L	ΔF_T	ΔF_L	ΔF_T	ΔF_L
$0.00 - 0.01$	10	5	8	5	1	1	13	7
$0.01 - 0.02$	3	4	5	3	1	2	5	5
$0.02 - 0.03$	1	2	3	2	1	1	4	3
$0.03 - 0.04$	2	2	3	2	0.7	0.8	4	3
$0.04 - 0.05$	1.0	1	1	0.8	0.6	0.7	2	1
$0.05 - 0.06$	0.8	0.6	1	0.8	0.4	0.4	2	1
$0.06 - 0.07$	0.7	0.4	1	0.7	0.4	0.4	1	0.9
$0.07 - 0.08$	0.5	0.3	0.8	0.5	0.2	0.2	1.0	0.6
$0.08 - 0.09$	0.5	0.2	0.5	0.3	0.2	0.2	0.8	0.5
$0.09 - 0.10$	0.4	0.2	0.5	0.3	0.2	0.2	0.7	0.4
$0.10 - 0.12$	0.4	0.1	0.4	0.2	0.1	0.1	0.5	0.3
$0.12 - 0.14$	0.3	0.1	0.3	0.2	0.08	0.09	0.4	0.2
$0.14 - 0.16$	0.2	0.07	0.1	0.06	0.08	0.09	0.3	0.1
$0.16 - 0.18$	0.2	0.1	0.1	0.09	0.01	0.01	0.3	0.1
$0.18 - 0.20$	0.2	0.07	0.07	0.05	0.03	0.03	0.2	0.08
$0.20 - 0.25$	0.1	0.02	0.05	0.03	0.02	0.02	0.1	0.04
$0.25 - 0.30$	0.07	0.009	0.03	0.01	0.009	0.010	0.08	0.02
$0.30 - 0.40$	0.04	0.008	0.05	0.006	0.008	0.009	0.07	0.02
$0.40 - 0.50$	0.02	0.011	0.03	0.016	0.009	0.010	0.04	0.02
$0.50 - 0.60$	0.006	0.003	0.003	0.003	0.0002	0.0002	0.007	0.005
$0.60 - 0.80$	0.005	0.003	0.004	0.003	0.0004	0.0004	0.007	0.004
$0.80 - 1.00$	0.002	0.001	0.002	0.001	0.0009	0.0011	0.003	0.002

Table 3: Main contributions to the systematic uncertainties on F_T and F_L, arising from variations of the track and event selection criteria, the angular range analysed and the influence of the region of $\lvert\cos\theta\rvert \approx 0$, together with the total systematic errors. Systematic uncertainties are correlated between x_p bins.

Criterion	$\Delta\frac{\sigma_T^{ch}}{\sigma_{tot}}$	$\Delta\frac{\sigma_L^{ch}}{\sigma_{tot}}$	$\Delta\langle n^{ch}\rangle$
Track and event selection	0.005	0.002	0.19
Angular range	0.004	0.003	0.05
Region of $\lvert\cos\theta\rvert \approx 0$	0.002	0.002	0.01
Weighting/fitting	0.001	0.0008	0.05
x_p evaluation method	0.001	0.0002	—
Uncertainty in K_s^0	—	—	0.02
Total	0.007	0.004	0.20

Table 4: Systematic deviations of the components of the charged particle cross-section and of the mean charged particle multiplicity due to variations of the specified criteria.

x_p range	$F_T^b(x_p)$	$F_L^b(x_p)$	$F_T^{uds}(x_p)$	$F_L^{uds}(x_p)$
$0.00-0.01$	$331 \pm 9 \pm 22$	$113 \pm 7 \pm 13$	$280 \pm 2 \pm 10$	$115 \pm 1 \pm 6$
$0.01-0.02$	$369 \pm 6 \pm 12$	$89 \pm 4 \pm 9$	$317 \pm 1 \pm 4$	$79 \pm 1 \pm 4$
$0.02-0.03$	$264 \pm 5 \pm 12$	$45 \pm 4 \pm 7$	$218 \pm 1 \pm 3$	$33.7 \pm 0.9 \pm 2.6$
$0.03-0.04$	$200 \pm 5 \pm 9$	$19 \pm 3 \pm 6$	$158.4 \pm 1.0 \pm 2.6$	$15.4 \pm 0.7 \pm 2.1$
$0.04-0.05$	$141 \pm 4 \pm 4$	$18 \pm 3 \pm 3$	$117.5 \pm 0.9 \pm 1.2$	$9.6 \pm 0.6 \pm 1.0$
$0.05-0.06$	$120 \pm 4 \pm 4$	$6 \pm 2 \pm 2$	$91.8 \pm 0.7 \pm 0.9$	$5.6 \pm 0.5 \pm 0.6$
$0.06-0.07$	$94 \pm 3 \pm 3$	$6 \pm 2 \pm 2$	$73.7 \pm 0.7 \pm 0.7$	$4.3 \pm 0.5 \pm 0.5$
$0.07-0.08$	$74 \pm 3 \pm 3$	$7 \pm 2 \pm 2$	$61.3 \pm 0.6 \pm 0.7$	$2.3 \pm 0.4 \pm 0.4$
$0.08-0.09$	$68 \pm 3 \pm 3$	$1 \pm 2 \pm 2$	$51.6 \pm 0.6 \pm 0.7$	$1.0 \pm 0.4 \pm 0.4$
$0.09-0.10$	$53 \pm 2 \pm 3$	$2 \pm 2 \pm 2$	$43.4 \pm 0.5 \pm 0.5$	$1.1 \pm 0.4 \pm 0.5$
$0.10-0.12$	$40 \pm 2 \pm 3$	$3 \pm 1 \pm 2$	$35.0 \pm 0.3 \pm 0.5$	$0.4 \pm 0.2 \pm 0.3$
$0.12-0.14$	$28 \pm 1 \pm 2$	$1.6 \pm 0.9 \pm 1.3$	$26.9 \pm 0.3 \pm 0.5$	$-0.3 \pm 0.2 \pm 0.3$
$0.14-0.16$	$19 \pm 1 \pm 1$	$1.7 \pm 0.7 \pm 0.7$	$20.5 \pm 0.3 \pm 0.4$	$0.02 \pm 0.19 \pm 0.16$
$0.16-0.18$	$15.9 \pm 1.0 \pm 1.1$	$0.4 \pm 0.7 \pm 0.7$	$15.9 \pm 0.2 \pm 0.3$	$0.32 \pm 0.17 \pm 0.19$
$0.18-0.20$	$11.2 \pm 0.8 \pm 1.1$	$0.8 \pm 0.6 \pm 0.9$	$13.7 \pm 0.2 \pm 0.3$	$-0.46 \pm 0.15 \pm 0.36$
$0.20-0.25$	$7.8 \pm 0.4 \pm 0.6$	$-0.2 \pm 0.3 \pm 0.2$	$9.4 \pm 0.1 \pm 0.2$	$-0.16 \pm 0.08 \pm 0.13$
$0.25-0.30$	$4.0 \pm 0.3 \pm 0.3$	$-0.03 \pm 0.20 \pm 0.11$	$5.92 \pm 0.09 \pm 0.10$	$-0.12 \pm 0.07 \pm 0.14$
$0.30-0.40$	$1.8 \pm 0.1 \pm 0.2$	$0.04 \pm 0.10 \pm 0.11$	$3.22 \pm 0.05 \pm 0.06$	$-0.10 \pm 0.03 \pm 0.11$
$0.40-0.50$	$0.44 \pm 0.07 \pm 0.07$	$0.13 \pm 0.05 \pm 0.19$	$1.42 \pm 0.03 \pm 0.06$	$-0.01 \pm 0.02 \pm 0.02$
$0.50-0.60$	$0.15 \pm 0.05 \pm 0.05$	$0.03 \pm 0.03 \pm 0.02$	$0.68 \pm 0.02 \pm 0.03$	$-0.02 \pm 0.02 \pm 0.02$
$0.60-0.80$	$0.04 \pm 0.02 \pm 0.03$	$0.001 \pm 0.012 \pm 0.018$	$0.24 \pm 0.01 \pm 0.01$	$-0.01 \pm 0.01 \pm 0.04$
$0.80-1.00$	$0.0002 \pm 0.0004 \pm 0.0004$	$-0.0001 \pm 0.0003 \pm 0.0001$	$0.024 \pm 0.004 \pm 0.004$	$0.005 \pm 0.003 \pm 0.004$
$\langle n^{ch} \rangle$	$23.47 \pm 0.07 \pm 0.36$		$20.35 \pm 0.01 \pm 0.19$	

Table 5: Transverse and longitudinal components of the fragmentation function for Z^0 decays into either $b\bar{b}$ or light quark-antiquark pairs The first error is statistical and the second one is systematic. The charged particle multiplicities are calculated by integrating the corresponding F_{T+L} distributions.

	Natural flavour mix		Flavour-tagged events	
	$\alpha_s^{LO} = 0.126,\ fixed$	$\alpha_s^{LO} = 0.131 \pm 0.066$	$\alpha_s^{LO} = 0.126,\ fixed$	$\alpha_s^{LO} = 0.133 \pm 0.032$
P_1	0.47 ± 0.07	0.46 ± 0.26	0.47 ± 0.05	0.46 ± 0.15
P_2	-2.90 ± 0.02	-2.85 ± 0.03	-2.84 ± 0.01	-2.84 ± 0.01
P_3	5 ± 1	4 ± 1	3.3 ± 0.5	3.5 ± 0.5
P_4	0.29 ± 0.01	0.30 ± 0.01	0.29 ± 0.01	0.30 ± 0.01
χ^2/ndf	$10/15 = 0.7$	$11/14 = 0.8$	$132/53 = 2.5$	$132/52 = 2.5$

Table 6: Parameters for the gluon fragmentation function (21) obtained from fits with α_s^{LO} either fixed at the value of 0.126 or treated as a free parameter. The *'Natural flavour mix'* columns correspond to the fit to the natural flavour mix data given in Table 1. The *'Flavour-tagged events'* columns correspond to the simultaneous fit to the b- and uds-tagged data given in Table 5 and the remaining untagged events.